E.O. Paton Electric Welding Institute of the National Academy of Sciences of Ukraine

International Scientific-Technical and Production Journal

The Paton WELDING JOURNAL

Issue 01 2018

Published Monthly Since 2000

English translation of the monthly «Avtomaticheskaya Svarka» (Automatic Welding) journal published in Russian since 1948

Address
E.O. Paton Electric Welding Institute,
International Association «Welding»
11 Kazimir Malevich Str. (former Bozhenko Str.),
03150, Kyiv, Ukraine
Tel.: (38044) 200 60 16, 200 82 77
Fax: (38044) 200 82 77, 200 81 45
E-mail: journal@paton.kiev.ua
www.patonpublishinghouse.com

State Registration Certificate
KV 4790 of 09.01.2001
ISSN 0957-798X
doi.org/10.15407/tpwj

Subscriptions
$348, 12 issues per year,
air postage and packaging included.
Back issues available.

CONTENTS

doi.org/10.15407/tpwj2018.01.01

EFFECT OF PARAMETERS OF ARC, LASER AND HYBRID METHODS OF WELDING ON STRUCTURE AND PROPERTIES OF BUTT JOINTS OF HIGH-STRENGTH STEEL S460M

V.D. POZNYAKOV, V.D. SHELYAGIN, S.L. ZHDANOV, A.V. BERNATSKY, A.A. MAKSYMENKO and **A.V. SIORA**
E.O. Paton Electric Welding Institute of the NAS of Ukraine
11 Kazimir Malevich Str., 03150, Kyiv, Ukraine. E-mail: office@paton.kiev.ua

The paper studies the effect of parameters of arc, laser and hybrid laser-arc welding on formation of structure and properties of weld metal and heat-affected zone of butt joints from high-strength low alloy steel S460M with yield point up to 480 MPa. It is shown that increase of rate of gas-shielded arc welding to 50 m/h (13.9 mm/s) allows receiving a quality weld with increased indices of static strength and impact toughness. Laser welding with increased cooling rate provokes reduction of the indices of ductility and impact toughness of weld metal that is related with formation of martensite hardening structure of weld metal and heat-affected zone of the welded joints revealing at higher cooling rate. Application of hybrid laser-arc welding method of steel S460M allows decreasing cooling rate of weld metal and heat-affected zone in comparison with laser welding method. This provides high level of mechanical properties and impact toughness of metal of these zones. 16 Ref., 1 Table, 5 Figures.

Keywords: *butt joints, high-strength steel, arc welding, laser welding, hybrid laser-arc welding, thermal cycle, structure peculiarities, mechanical properties*

Mechanized and automatic arc welding in active shielding gases medium as well as in their mixtures with inert gas (Ar + CO_2, Ar + CO_2 + O_2) [2] using solid wire as well as flux-cored wire [3] are widely applied in manufacture of metallic structures of high-strength steels [1] of up to 10 mm thickness. Preferable, from point of view of receiving of quality welded joints are such modes of arc welding, at which weld metal and metal of heat-affected zone (HAZ) preserve the strength, ductility and cold resistance at the level of base metal and have high resistance to cold crack formation [4].

Laser [5, 6] and hybrid laser-arc welding [7–16] are implemented in production in the recent years in order to decrease deformation and increase of quality of welded thin-wall (thickness up to 10 mm) metallic structures of ferrite-pearlite class low-alloy steels. The advantages of these types of welding are [5–16]: increase of productivity due to several times rise of welding rate [7]; significant decrease of heat input [8, 9]; obtaining the balanced fine-grain microstructures in weld metal and HAZ [10–12], which exceed joint strength, reduce level of residual stresses and susceptibility to cold crack formation [13–15].

In this connection the relevant are the investigations of effect of technological processes parameters in laser, arc and hybrid laser-arc welding on structure and properties of butt welded joints from low-alloy steels of C440–C460 strength class.

Present work has studied the effect of parameters of arc, laser and hybrid laser-arc welding on formation of structure as well as properties of weld metal and HAZ of joints of high-strength alloy steel S460M with yield point σ_y = 480 MPa and following composition, wt.%: 0.15 C; 0.23 Si; 1.3 Mn; 0.09 Cr; 0.02 Ni; 0.23 Mo; 0.1 V; 0.6 Cu; 0.013 S; 0.017 P.

An initial stage of work was dedicated to investigation of effect of mode parameters of mentioned above welding methods on heating and cooling conditions of butt welded joints of 8 mm thickness.

Automatic arc welding of such joints is carried out by flux-cored wire Megafil 821R of 1.2 mm diameter in gas mixture (82 % Ar + 18 % CO_2) at the following modes, i.e. welding current I_w = 220–240 A; arc voltage U_a = 30–32 V; welding rate v_w = 30; 40; 50 m/h (8.3, 11.1 and 13.9 mm/s, respectively). Further increase of welding rate appeared to be unreasonable, since selected welding modes did not allow getting quality joints. Weld formation was deteriorated, lack of penetration and spattering of electrode metal appeared.

In laser process the welding rate lied in the limits from 40 m/h (11.1 mm/s) to 50 m/h (13.9 mm/s) ($w_{6/5}$ = 65–103 °C/s). The parameters of laser radia-

tion were 4.4 kW power of Nd:YAG laser, focus penetration ΔF = –1.5 mm.

In hybrid laser-arc welding the modes of laser constituent were 4.4 kW power of Nd:YAG laser, focus penetration ΔF = –1.5 mm. The parameters of arc constituent of hybrid welding process at constant consumption of shielding gas mixture 82 % Ar + 18 CO_2 Q_{shield} = 14–16 l/min varied depending on welding rate. At rate of hybrid laser-arc welding v_w = 72 m/h (20.0 mm/s) current and arc voltage made I_w = 120 A and U_a = 22 V; at that I_w = 170 A and U_a = 24 V at welding rate v_w = 90 m/h (25 mm/s) and I_w = 200 A at v_w = 110 m/h (30.5 mm/s).

Record of thermal welding cycles was carried out using chromel-alumel thermal couples of 0.5 mm diameter, connected through USB-converter of electric signals to PC. Their joint was located in the place of HAZ metal overheating. Cooling rate of HAZ metal in a 600–500 °C ($w_{6/5}$) temperature range was taken as a parameter of thermal cycle, which further was used as criterion for evaluation of its effect on structure and mechanical properties of weld metal and HAZ of welded joints.

Analysis of thermal cycles of automatic arc welding of S460M steel butt joints showed that a heating rate of such joints virtually does not depend on rate of heat source — welding arc displacement and makes 180–200 °C/s. Intensity of HAZ metal cooling (Figure 1) has significant effect on welding rate. Increase of v_w promotes rise of cooling rate of welded joints. Thus, cooling of metal of HAZ overheating area in the 600–500 °C temperature range at welding rate v_w = = 30 m/h (8.3 mm/s) takes place with $w_{6/5}$ = 24 °C/s rate, at v_w = 40 m/h (11.1 m/s) $w_{6/5}$ = 27 °C/s and at arc welding rate v_w = 50 mm/h (13.9 mm/s) HAZ metal is cooled with $w_{6/5}$ = 36 °C/s rate.

Analysis of thermal cycles of laser and hybrid laser-arc welding of butt joints of S460M steel showed that the values of heating rates of HAZ metal to 1100–1300 °C temperatures and cooling rates of the overheating areas in 600–500 °C temperature range are identical to the values received for steel 14KhGN2MDAFB [13].

From point of view of structure formation laser welding process is characterized by «rigid» thermal cycle with sufficiently high (up to $w_{6/5}$ = 103 °C/s) cooling rates in HAZ metal of S460 steel welded joints that can result in formation in it of hardening structures of high hardness. It is shown by the results of investigations of structural transformations in HAZ metal of S460M steel in heating-cooling process, obtained with the help of dilatometry [16]. For «softening» of such thermal cycle it is reasonable to use hybrid laser-arc welding, which allows providing

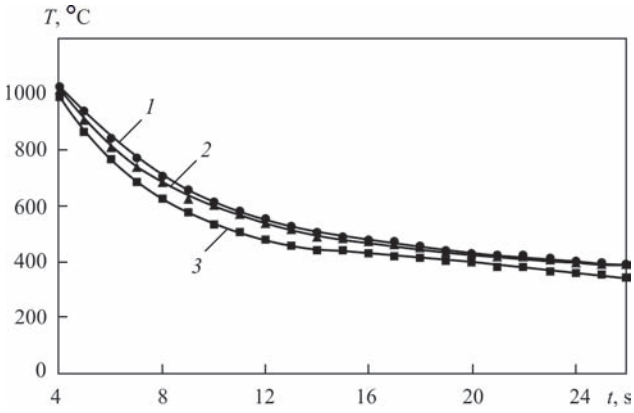

Figure 1. Thermal cycles in automatic arc welding of S460M steel: *1* — v_w = 30 m/h ($w_{6/5}$ = 24 °C/s); *2* — 40 m/h (27 °C/s); *3* — 50 m/h (36 °C/s)

cooling of HAZ metal of welded joints with $w_{6/5}$ = 58–62 °C/s rate at productivity preserving.

Differences in cooling conditions in arc, laser and hybrid laser-arc welding cause formation of different structure that, in turn, results in change of mechanical properties of weld metal and HAZ of welded joints. It is indicated by the results of investigations carried below.

Based on data of metallographic analysis it is determined that microstructure of HAZ metal of specimens of steel S460M performed by arc welding can vary from ferrite to bainite. Increase of cooling rate from $w_{6/5}$ = 24 °C/ s (v_w = 30 m/h, Figure 2, *a*) to $w_{6/5}$ = = 27 °C/ s (v_w = 40 m/h, Figure 2, *b*) and $w_{6/5}$ = 36 °C/s (v_w = 50 m/h, Figure 2, *c*) promotes structure transformation from acicular ferrite into bainite and it consists of different-oriented packages of bainite containing residual austenite. At that value of integral microhardness in HAZ metal of S460M specimens rises (from *HV*0.1-2490–2730 MPa at v_w = 30 m/h to *HV*0.1-3530–3650 MPa at v_w = 50 m/h, respectively).

Transformation of the structure from bainite to martensite (Figure 3) is observed for specimens cooling rate $w_{6/5}$ around 60 °C/s, typical for hybrid laser-arc welding, in HAZ metal of welded joints of S460M steel. This cooling rate is characterized with acicular martensite structure with different-oriented needles of 60 and 120 ° angle. HAZ metal structure contains dark and light etching martensite. In this case microhardness of dark etching martensite makes *HV*0.1-3600–3760 MPa, and that for light etching is *HV*0.1-3860–4260 MPa.

Increase of cooling rate for more than 100 °C/s (typical for laser welding with v_w = 50 m/h) also promotes formation of martensite in HAZ metal of S460M steel welded joints. But under such conditions of cooling the martensite structure consists of more close-packed packages that results in further growth of microhardness values *HV*0.1-4100–4630 MPa.

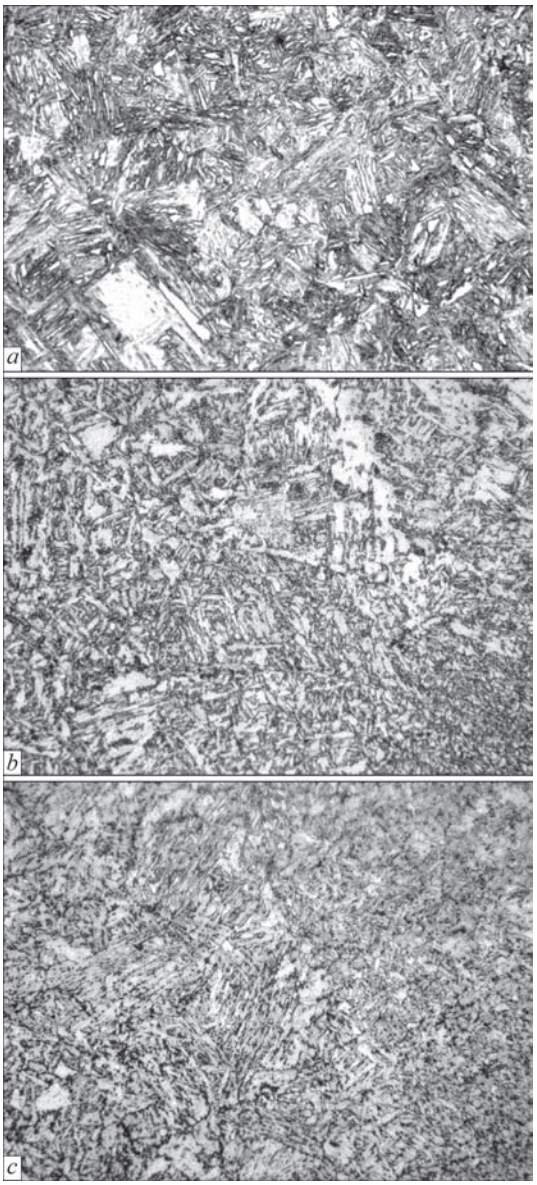

Figure 2. Microstructure (×500) of HAZ metal of steel S460M welded joints produced at different rate of arc welding: *a* — v_w = = 30 m/h (8.3 mm/s) ($w_{6/5}$ = 24 °C/s); *b* — 40 m/h (11.1 mm/s) ($w_{6/5}$ = 27 °C/s); *c* — 50 m/h (13.9 mm/s) ($w_{6/5}$ = 36 °C/s)

The specimens for static tension tests (type I) and V-notch impact bend tests (type X) on weld metal as well as HAZ were made from welded joints according to GOST 6996–66 for evaluation of mechanical properties. The tensile specimens were tested at room temperature and the impact bend ones at temperatures from 20 to –40 °C.

The results of investigation of mechanical properties of welded joints, performed using arc, laser and hybrid laser-arc welding are given in the Table.

It is determined that in increase of arc welding rate from 30 m/h ($w_{6/5}$ = 24 °C/ s) to 50 m/h ($w_{6/5}$ = = 36 °C/s) the values of yield point and ultimate strength rise from 582 to 607 MPa and from 625 to 657 MPa, respectively. Impact toughness of weld metal and HAZ of welded joints at that also increases. The

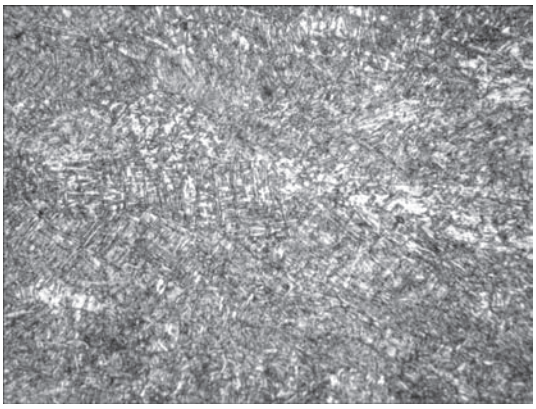

Figure 3. Microstructure (×500) of HAZ metal in hybrid laser-arc welding of S460M steel (v_w approximately 90 m/h (25.0 mm/s))

most significant increase of *KCV* indices is observed in the specimens which were tested at –40 °C temperature. In particular, rise of $w_{6/5}$ from 24 (v_w = 30 m/h) to 36 °C/ s (v_w = 50 m/h) increases the values of weld metal KVC_{-40} from 70–83 to 137–161 J/cm^2 and HAZ from 80–110 to 115–120 J/cm^2. Weld metal ductility of such joints, independent on selected welding conditions, virtually does not change and remains at high level (elongation 21–23 % and reduction in area 68–70 %).

The results of mechanical tensile tests of the cylinder specimens showed that yield point and tensile strength of weld metal of S460M welded joints, produced using laser process, rises two times in comparison with welded joints, produced by arc welding. However, its ductility is significantly reduced at that, namely two times at welding rate 40 m/h and virtually four times at v_w = 50 m/h. Impact toughness of weld metal of such joints completely satisfies the requirements set for welded joints of steels with $\sigma_{0.2} \geq$ $\geq$ 390 MPa ($KVC_{-40} \geq$ 34 J/cm^2). At the same time, it is noted that increase of rate of laser welding reduces the indices of impact toughness of weld metal of S460M steel welded joints at positive as well as at negative temperatures. Impact toughness of HAZ metal of such welded joints lies at high level (KCV_{40} = = 120–150 J/cm^2), and its values in the investigated range of welding rates virtually do not change. Hybrid laser-arc welding of S460M steel demonstrates the same tendency of change of mechanical properties of weld metal as in laser welding. Static strength of weld metal of S460M steel welded joints rises in comparison with arc welding per 65–70 %, however, its ductility reduces virtually two times.

Increase of rate of hybrid laser-arc welding to 110 m/h ($w_{6/5}$ = 58–63 °C/s) results in reduction of the strength indices by 100 MPa and insignificant (by 15 %) rise of the ductility indices (Table). Increase of rate of hybrid laser-arc welding from 72 (20.0 mm/s) to 110 m/h (30.5 mm/s) ($w_{6/5}$ = 58–63 °C/s) promotes decrease of

Mechanical properties of S460M steel welded joints in arc, laser and hybrid laser-arc welding

Variant of welding	$\sigma_{0.2}$, MPa	σ_t, MPa	δ_5, %	ψ, %	*KCV*, J/cm² at *T*, °C					
					Weld			HAZ		
					20	–20	–40	20	–20	–40
Base material	490	600	24	59	110*	–	–	–	–	–
Arc v_w = 30 m/h (8.3 mm/s)	576.3 587.3	623.6 626.3	22.3 23.3	69.7 68.0	186.0 172.1	121.7 153.7	69.8 83.4 80.9	–	–	83.3 109.4 90.7
Arc v_w = 40 m/h (11.1 mm/s)	586 608.9	629.6 637.7	21.7 23.3	69.8 69.9	176.2 173.9	158.3 134.8	93.3 80.1 113.9	–	–	107.1 73.6 88.6
Arc v_w = 50 m/h (13.9 mm/s)	606.4 608.3	658.1 656.7	21.0 23.0	68.0 69.9	174.8 185.7	149.0 167.9	161.1 145.2 136.9	–	–	120.8 120.2 115.2
Laser v_w = 40 m/h (11.1 mm/s)	998.8 996.0 997.4	1172.2 1151.4 1161.8	10.0 11.3	24.9 41.2	175.1 202.3	163.7 232.1 112.3	109.4 113.2 132.7	100.8 207.0	–	130.5 116.9 148.6
Laser v_w = 50 m/h (13.9 mm/s)	964.6 923.3 907.7	1123.1 1130.0 1068.3	5.3 6.7 4.0	19.5 19.5 18.5	154.2 87.6	57.2 85.2 54.2	46.0 102.5 42.3	150.0	–	167.5 132.1 157.2
Hybrid v_w = 72 m/h (20.0 mm/s)	861.3 795.1	1047.3 971.5	11.3 8.0	34.0 36.4	116.5 103.2	123.1 103.4 103.4	67.6 101.5 96.5	33.8 106.6 58.3	–	45.0 42.1 40.8
Hybrid v_w = 90 m/h (25.0 mm/s)	826.8 800.9	1033.5 1019.9	12.0 9.4	41.6 41.8	109.5 125.7	92.4 71.0 111.2	79.3 76.8 60.5	92.5 119.9 136.3	–	67.5 85.7 96.8
Hybrid v_w = 110 m/h (30.5 mm/s)	745.1 638.1	941.9 894.7	13.3 12.9	46.2 46.4	58.9 77.4	39.7 58.4 55.7	57.3 44.4 60.8	114.9 128.2 121.5	123.9 125.7 124.8	46.9 59.1 101.6

*Data of base metal across rolled stock.

impact toughness of weld metal at all test temperatures (KCV_{20} from 189 to 102 J/cm², KCV_{-20} from 170 to 75 J/cm² and KCV_{-40} from 118 to 63 J/cm²).

Resistance to cold crack formation in S460M steel welded joint, performed using arc, laser and hybrid laser-arc welding processes, were evaluated using technological test «rigid boxing» [13]. A reference welded joint was of B = 100 mm width that corresponded to the highest rigidity of the planes fixed on a plate. It is determined as a result of such investigations that S460M steel welded joints performed using arc, laser and laser-arc processes are not susceptible to formation of cold cracks. This conclusion was made based on the results of analysis of the macrosections made of technological tests of Figure 4, *a–c*. It showed that there are no cold cracks in the joints even in welding without preheating.

In addition to cold cracks a welded joint can have other defects such as lacks of penetration, pores, undercuts, slag inclusions etc. At static and cyclic loading they can play a role of nucleus of initiation and propagation of cracks, which during operation (in particular at negative temperatures) can result in brittle fracture of metal. Therefore, further work was directed on evaluation of resistance of weld metal and HAZ of S460M steel welded joints to brittle fracture. These investigations were carried out using criteria of fracture mechanics. The double-sided single-pass joints of S640M steel of 10 mm thickness with groove preparation were made for these purposes using arc welding process and that without groove preparation was made by hybrid laser-arc welding. Arc welding of such joints was performed at 30 m/h rate and hybrid laser-arc welding at 72 m/h rate. The rest of technological parameters of welding modes are indicated above. The indicated welded joints were used to make the specimens of 20×10 mm section for three point bend tests. A chevron notch on the specimens was done in such a way that a mouth of crack grown from its tip was in a weld metal (part of specimens) and in joint fusion line (other part of the specimens). The specimens were tested at –40, –20 and 20 °C temperatures. The results of tests were used for determination of critical coefficient of stress intensity K_{1C} and critical crack opening δ_C.

Analysis of the results of carried investigations allowed determining the following. Steel S460M welded joints made by arc welding differ by higher brittle crack resistance. At test temperatures –40, –20 and 20 °C the average K_{1C} values of weld metal of such

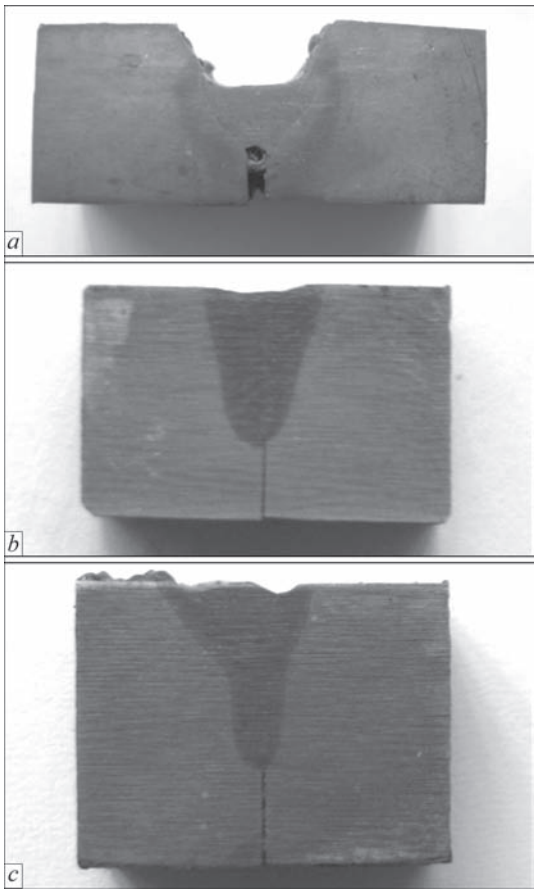

Figure 4. Macrosections of rigid butt technological probes of S460M steel of 8 mm thickness (B — 100 mm): *a* — in automatic arc welding in Ar + 18 % CO_2 gas mixture with flux-cored wire Megafil 821R (v_w = 30 m/h (8.3 mm/s)); *b* — laser welding without filler material (v_w = 40 m/h (11.1 mm/s)); *c* — in hybrid laser-arc welding with indicated above flux-cored wire (v_w = 72 m/h (20.0 mm/s))

joints make 86.3; 96.8 and 101 MPa√m, respectively (Figure 5, *a*). Increase of test temperatures promote also rise of δ_C indices of weld metal from 0.08 and 0.09 mm at –40 and –20 °C temperatures, respectively, to 0.12 mm at 20 °C test temperature (Figure 5, *b*).

High, but significantly lower in comparison with the weld, produced by arc welding, K_{1C} indices are typical for the welded joints, made using hybrid laser-arc welding. Average K_{1C} indices rise from 52.2 MPa√m (test temperature –40 °C) to 55.4 and 81.2 MPa√m at test temperatures –20 and 20 °C, respectively, (Figure 5, *a*) with rise of test temperature of specimens, produced from such joints. δ_C indices of weld metal are changed in the same way from 0.067 mm to 0.076 mm at –40, and –20 °C temperatures, respectively, and to 0.1 mm at test temperature 20 °C (Figure 5, *b*).

The following can be noted in relation to HAZ metal of welded joints from investigated steel. At test temperature 20 °C the values of K_{1C} and δ_C indices of HAZ metal of welded joints made by arc as well as hybrid laser-arc welding are close and, correspondingly

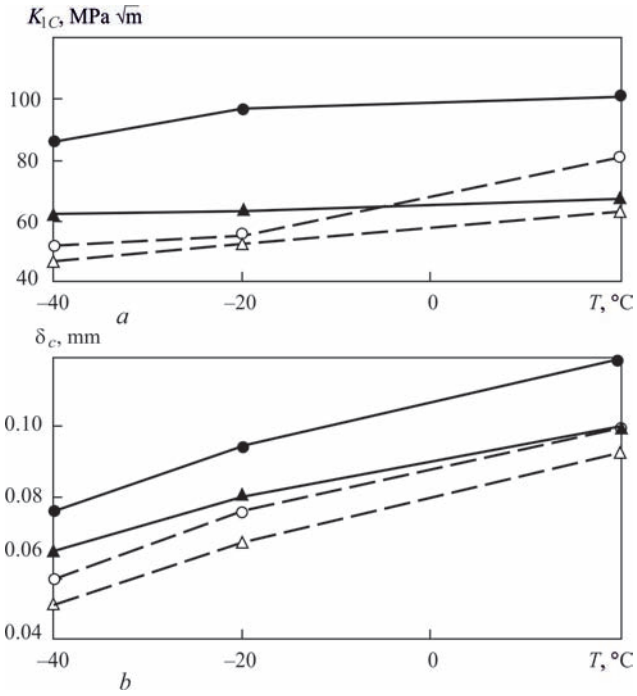

Figure 5. Dependence of values of critical coefficient of stress intensity K_{1C} (*a*) and critical crack opening δ_C (*b*) on tests temperature for weld metal (●, ○) and HAZ metal (▲, Δ) of δ = 8 mm S460M steel welded joints in automatic arc (●, ▲) and hybrid laser-arc welding (○, Δ)

make 65.6 MPa√m and 0.095 mm. Under conditions of testing at negative temperatures the values of K_{1C} and δ_C of HAZ metal of welded joints, produced using hybrid laser-arc welding, are 22–32 % lower than in the welded joints made using arc welding. Thus, at –20 ° C test temperature the K_{1C} and δ_C indices of HAZ metal of welded joints, performed by hybrid laser-arc welding, make 52.6 MPa√m and 0.057 mm, and that for arc welding is 63.3 MPa√m and 0.076 mm. At specimen test temperature –40 °C K_{1C} and δ_C indices of HAZ metal of joins are K_{1C} = 46.7 MPa√m and δ_C = 0.05 mm in welded joints produced by hybrid laser-arc welding and 62.1 MPa√m, δ_C = 0.065 mm, made by arc welding (Figure 5, *a*, *b*).

S460M steel welded joints, performed using arc and hybrid laser-arc welding, differ on resistance to fatigue crack formation. It is shown by the results of cyclic cantilever bend tests of specimens. Such tests were carried out applicable to the specimens of 400×120×10 mm size, produced of butt joints, arc and hybrid welding of which was carried out in shielding gas mixture 82 % Ar + 18 % CO_2 using Megafil 821R wire of 1 mm diameter at modes similar to modes for brittle fracture test joints. The tests of specimens at symmetric cyclic loading were carried out with 14 Hz cycle frequency. Cycle stress varied from 40 to 80 MPa with 20 MPa step. The results of carried investigations showed that the arc welded joints have higher resistance to formation of fatigue cracks.

Under indicated conditions of loading, formation of fatigue cracks in the arc welded joints were not observed after $N = 2 \cdot 10^6$ cycles of loading. The fatigue cracks of 3 mm depth were detected only in the welded joints performed by hybrid laser-arc process at cycle stresses 60 and 80 MPa. Thus, in the specimens, which were tested at 60 MPa cycle stress, they started to be formed after 1540400 cycles of loading, and at σ = 80 MPa after N = 1300680 loading cycles.

Conclusions

Increase of welding rate of gas-shielded arc welding up to v_w = 50 m/h (13.9 mm/s) ($w_{6/5}$ = 36 °C/s) allows receiving quality weld in welded joints of high-alloy S460M steel with yield point σ_y = 480 MPa and increased indices of static strength and impact toughness.

In laser welding rise of cooling rate $w_{6/5}$ of S460M steel welded joints promotes decrease of indices of ductility and impact toughness of weld metal. It is related with formation of martensite hardening structure in weld metal and HAZ of welded joints, which is formed as a result of typical for laser welding intensive cooling of metal in 600–500 °C temperature range ($w_{6/5}$ = 65–103 °C/s).

Application of hybrid laser-arc welding of S460M steel allows significantly rising linear welding rate in comparison with arc and laser processes. At that decrease of cooling rate of weld metal and HAZ is provided in comparison with laser welding method. All together it allows significantly rising productivity of welding process and preserving at that indices of mechanical properties and impact toughness of weld metal and HAZ of the welded joints at the level of the requirements made to welded structures produced of steels of C440–C490 strength class.

It is determined that S460M steel welded joints produced using arc, laser and hybrid laser-arc processes, are not susceptible to cold crack formation.

The indices of fracture toughness of joints in hybrid laser-arc welding can be increase due to formation in HAZ metal of lower bainite structure that is reached at welding rate 72 m/h.

It is shown that butt joints of S460M steel, produced by arc welding method, have higher service life. In hybrid laser-arc welding fatigue fracture resistance can be increases under condition of performance of groove preparation in the joints with small opening angle up to 10°.

1. Odessky, P.D., Molodtsov, A.F., Morozov, Yu.D. (2011) New effective low-alloy steels for building metallic structures. *Montazhnye i Spetsialnye Raboty v Stroitelstve*, **5**, 20–25 [in Russian].
2. Bilyk, A.S., Kurashev, R.V., Gorbatenko, V.V. et al. (2013) Application of thermomechanically hardened rolled sheet in welded metallic structures. *Promyslove Budivnytstvo ta Inzhenerni Sporudy*, **4**, 2–5 [in Russian].
3. Poznyakov, V.D., Zhdanov, S.L., Zavdoveev, A.V. et al. (2016) Weldability of high-strength microalloyed steel S460M. *The Paton Welding J.*, **12**, 21–28.
4. Ufuah, E. (2013) Elevated temperature mechanical properties of butt welded connections made with high-strength steel grades S355 and S460M. In: *Proc. of Int. Conf. on Design, Fabrication and Economy of Metal Structures* (Miscolc, Hungary, April 24–26, 2013), 407–412.
5. Grigoryants, A.G., Grezev, V.A. (2015) Special features of laser welding using fibre and CO_2 lasers. *Welding Int.*, 29(**12**), 968–973.
6. Markovits, T., Takacs,J. (2010) Edge welding of laminated steel structure by pulsed Nd:YAG laser. *Physics Procedia*, **5**, Pt B, 47–52.
7. Moore, P.L., Howse, D.S., Wallach, E.R. (2004) Microstructures and properties of laser/arc hybrid welds and autogenous laser welds in pipeline steels. *Sci. and Techn. of Welding and Joining*, 9(**4**), 314–322.
8. Kah, P., Salminen, A., Martikainen, J. (2010) Laser-arc hybrid welding processes (Review). *The Paton Welding J.*, **6**, 32–40.
9. Atabak, M., Ma, J., Yang, G., Kovacevic, R. (2014) Hybrid laser/arc welding of advanced high-strength steel in different butt joint configurations. *Materials & Design*, **64**, 573–587.
10. Gu, X.Y., Duan, Z.Z., Gu, X.P. et al. (2015) Microstructure and mechanical properties of laser-MAG hybrid welded thick-section weathered steel joint. *Int. J. Adv. Manuf. Technol.*, 81(**5**), 825–831.
11. Cao, X., Wanjara, P., Huang, J. et al. (2011) Hybrid fiber laser-arc welding of thick section high-strength low-alloy steel. *Materials & Design*, 32(**6**), 3399–3413.
12. Kelly, S.M., Brown, S.W., Tressler, J.F. et al. (2009) Using hybrid laser-arc welding to reduce distortion in ship panels. *Welding J.*, 88(**3**), 32–36.
13. Poznyakov, V.D., Shelyagin, V.D., Zhdanov, S.L. et al. (2015) Laser-arc welding of high-strength steels with yield strength of more than 700 MPa. *The Paton Welding J.*, **10**, 19–24.
14. Berdnikova, O., Poznyakov, V., Bushma, O. (2016) Laser and hybrid laser-arc welding of high strength-steel N-A-XTRA-70. *Mat. Sci. Forum*, **870**, 630–635.
15. Berdnikova, O., Sydoretz, V., Alekseienko, T. (2014) Structure and properties of laser-welded joints from high-strength steels. *Appl. Mech. Mater.*, **682**, 240–245.
16. Grigorenko, G.M., Poznyakov, V.D., Zuber, T.A. et al. (2017) Peculiarities of formation of structure in welded joints of microalloyed structural steel S460M. *The Paton Welding J.*, **10**, 2–8.

Received 27.11.2017

doi.org/10.15407/tpwj2018.01.02

RESISTOMETRIC METHOD OF WELDING SPEED MEASUREMENT FOR SIMULATING WELDING SYSTEMS

L.M. LOBANOV[1], **N.M. MAKHLIN**[2], **A.E. KOROTYNSKY**[1], **V.Yu. BURYAK**[2] and **A.G. SIPARENKO**[2]
[1]E.O. Paton Electric Welding Institute of the NAS of Ukraine
11 Kazimir Malevich Str., 03150, Kyiv, Ukraine. E-mail: office@paton.kiev.ua
[2]SE «Scientific and Engineering Center of Welding and Control in the Field of Nuclear Engineering»
of the E.O. Paton Electric Welding Institute of the NAS of Ukraine
11 Kazimir Malevich Str., 03150, Kyiv, Ukraine. E-mail: electro@paton.kiev.ua

Some theoretical problems of resistometric method for determination of welding arc spot coordinates and evaluation of speed of electrode movement during realization or simulation of arc welding, as well as the peculiarities of plotting the hardware part and software of simulating welding systems using this method are considered. The examples of application this method in the hardware-software complexes (welding simulators), as well as the basic variants of schematic and technical construction of devices for realization of resistometric method in the simulating welding systems, designed and industrially manufactured at the SE «Scientific and Engineering Center of Welding and Control in the Field of Nuclear Engineering» (SEC WCNE) of the E.O. Paton Electric Welding Institute of the NAS of Ukraine are presented. 17 Ref., 4 Figures.

Keywords: *arc spot coordinates, welding speed, simulating welding systems, simulator of workpiece welded, welding speed control devices, welding current sensors, «current loop»*

In the process of development of works on designing the simulating welding systems (SWS), different methds for welding speed estimation and devices for realizing these methods were proposed [1-3]. In the opinion of many authors, to estimate the welding speed in arc SWS, the technical means applying video sensors [4], devices of acoustic location [5], receivers of optical [6–8] or thermal radiation [1, 9, 10] are most acceptable.

Obviously, the use of video sensors provides the welding speed measurement with a high accuracy, but at the same time today the complexity and cost of hardware and software means of SWS are increasing, which is economically unreasonable in the vast majority of cases.

The use of acoustic location methods in arc SWS (especially in low-amperage ones) is rather complicated due to the low level of useful signals of the arc simulator [11] and, therefore, it is little promising.

For welding speed control devices (WSCD), designed using discrete sensitive elements which perceive optical radiation of visible or infrared range from the moving arc, the dependence on optical state of surrounding medium is characteristic, whereas WSCD on the basis of thermosensors are characterized by dependence on geometric shape of surrounding bodies and distance from them to thermosensors, as well as on the temperature and heat conductivity of the surrounding medium. In addition to a comparatively low accuracy of measurements, among the disadvantages of WSCD produced on receivers of optical or thermal radiation, the need in schematic-design complications of both hardware interface of SWS, as well as the manipulator-positioner and simulators of welding tools or workpiece welded, being in its composition, should be mentioned.

The analysis of capabilities of the known methods of WSCD and increasingly growing technological and didactic requirements to arc SWS shows that the most known and existing WSCD are already far from fully meeting these requirements.

Meanwhile, in arc SWS, quite satisfactory results can be achieved by using a relatively easy realizable resistometric method for determination of moving arc coordinates and estimating the welding speed. This method is based on the method of determining coordinates of a measuring probe in a conductive medium [12, 13], which was developed by V.V. Vasiliev and L.A. Simak at the G.E. Pukhov Institute for Problems of Modeling in Power Engineering of the NAS of Ukraine and later found development at the E.O. Paton Electric Welding Institute (PWI) and SEC WCNE for systems of monitoring the arc welding processes and SWS as-applied to the moving spot of welding arc or its simulator.

The principle of resistometric method is explained by Figure 1.

The simulator of workpiece welded (SWW), typical for SWS, represents a steel plate of rectangular shape, the length of which is l_0, the width is d_0 and the thickness is δ_0, moreover, $\delta_0 << d_0 << l_0$. One of the output poles of the welding power source G is connected to the point of connection of two branches (*ac* and *bc*), each of them is connected to one of two current (*a* or *b*) conductors by the second point, on the opposite end sides of SWW. The second output pole of the welding power source is connected to the current conductors of simulator of the welding tool (electrode holder).

When using the welding source in the mode of the current source (stabilizer), which is characterized by a «bayonet» external volt-ampere characteristic (which is in the most SWS), the welding current I_a does not depend on voltage drops at the arc, in SWW, in the wires and current conductors of the welding circuit.

From the obvious equality $R_0 = R_1 + R_2$ (where R_0 is the electrical resistance of SWW, R_1, R_2 are the resistances of its regions *ax* and *bx*, respectively) and from the assumption about inalterability of SWW section along its entire length l_0 it comes out that the coordinate *x* of the arc spot on SWW is determined by the relation:

$$x = l_0 R_1/R_0 = l_0(1 - R_2/R_0). \quad (1)$$

In accordance with the laws of Kirchhoff and assumptions that the electrical resistances of SWW and its individual regions remain unchanged in the process of welding, and the electrical resistances of branches *ac* and *bc* are equal between each other and are negligibly small as compared to the resistance of SWW, for regions *cax* and *cbx* the following system of equations is justible:

$$\begin{cases} I_1 + I_2 = I_a \\ I_1 R_1 = I_2 R_2 \end{cases}, \quad (2)$$

where I_1, I_2 are the currents passing through the regions *cax* and *cbx*, respectively.

The solution of the system of equations (2), taking into account the expression (1) is the following relations:

$$I_1 = I_a(1 - x/l_0), \quad (3)$$

$$I_2 = I_a x/l_0, \quad (4)$$

from which we obtain the expression for the arc spot coordinate *x*:

$$x = l_0(1 - I_1/I_a) = l_0 I_2/I_a, \quad (5)$$

and from it the expression for the speed of arc movement (welding speed) V_w is obtained:

$$V_w = dx/dt = l_0/I_a(-dI_1/dt) = l_0/I_a dI_2/dt. \quad (6)$$

Thus, the solution of the problem on estimation of welding speed in SWS is reduced to determining the changes in time of currents in the branches, by which SWW is connected to one of the output poles of the welding power source.

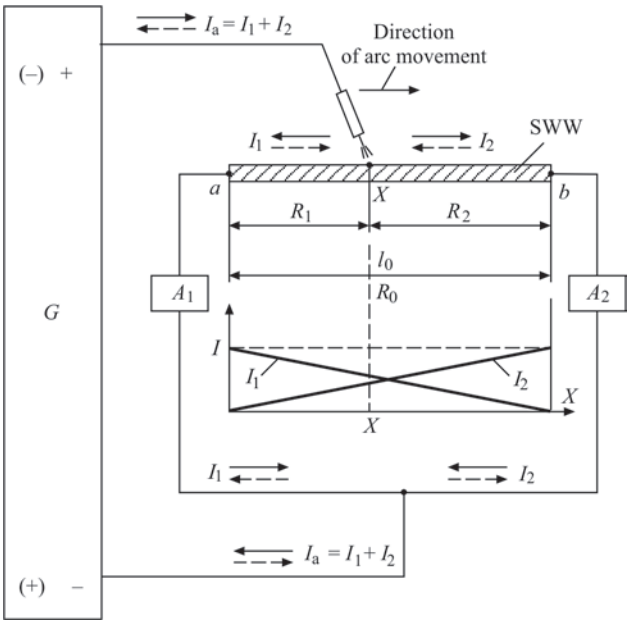

Figure 1. Scheme of resistometric method for determining welding arc spot coordinate and measuring welding speed in SWS (description see in the text: A_1, A_2 are the current sensors in the branches *cax* and *cbx* of the welding circuit)

The real connections of SWW with a welding circuit are carried out by conductors having a finite length and a certain section, and, consequently, having an ohmic resistance.

Figure 2 shows an equivalent diagram of welding circuit in which resistors R_1^* and R_2^* imply the active resistances of branches *ac* and *bc*. Obviously, taking into account R_1^* and R_2^*, the system of equations for the regions *cax* and *cbx* has the following form:

$$\begin{cases} I_1^* = I_2^* = I_a \\ I_1^*(R_1 + R_1^*) = I_2^*(R_2 + R_2^*) \end{cases}, \quad (7)$$

where I_1^*, I_2^* are the currents through the real regions *cax* and *cbx*.

Solving the system of equations (7), we obtain the expressions:

for currents I_1^*, I_2^*:

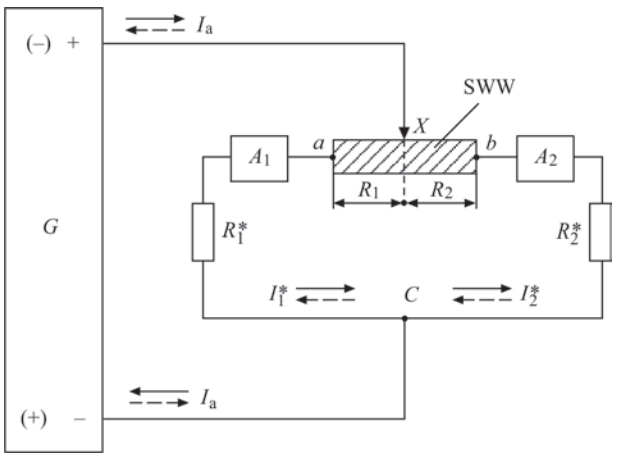

Figure 2. Equivalent electric diagram of SWS welding circuit (description see in the text)

$$I_1^* = \frac{I_a(R_2 + R_2^*)}{R_0 + R_1^* + R_2^*}, \quad (8)$$

$$I_2^* = \frac{I_a(R_1 + R_1^*)}{R_0 + R_1^* + R_2^*}; \quad (9)$$

for arc spot coordinate:

$$x^* = l_0\left[\left(1+\frac{R_2^*}{R_0}\right) - \frac{I_1^*}{I_a}\left(1+\left(R_1^* + \frac{R_2^*}{R_0}\right)\right)\right] = l_0\left[\frac{I_2^*}{I_a}\left(1+\left(R_1^* + \frac{R_2^*}{R_0}\right) - \frac{R_1^*}{R_0}\right)\right]; \quad (10)$$

for welding speed:

$$V_w^* = \frac{l_0}{I_a}\left(1+\frac{R_1^* + R_2^*}{R_0}\right)\left(-\frac{dI_1^*}{dt}\right) = \frac{l_0}{I_a}\left(1+\frac{R_1^* + R_2^*}{R_0}\right)\frac{dI_2^*}{dt}. \quad (11)$$

Here:

$$\frac{dI_1^*}{dt} = \left(\frac{1}{1+\frac{R_1^* + R_2^*}{R_0}}\right)\frac{dI_1}{dt}, \quad (12)$$

$$\frac{dI_2^*}{dt} = \left(\frac{1}{1+\frac{R_1^* + R_2^*}{R_0}}\right)\frac{dI_2}{dt}, \quad (13)$$

By making simple transformations with the substitution of expressions (8) and (9) into (10), and expressions (12) and (13) into (11), it is easy to be sure that $x^* = x$, and $V_w^* = V_w$, and, consequently, the active resistances R_1^* and R_2^* of branches *ac* and *bc* of the welding circuit do not influence the determination of arc spot coordinate and welding speed. At the same time, it follows from the expressions (8), (9), (12) and (13) that on the values of relation $(R_1^* + R_2^*)/R_0$ the values of currents I_1^*, I_2^* and their derivatives dI_1^*/dt and dI_2^*/dt depend.

On the relation $(R_1^* + R_2^*)/R_0$, the characteristic largely depends, which is important for realization of resistometric method, which can be called the sensitivity by the current E_i, and determined through the values of currents I_1^*, I_2^* per unit of length of SWW according to the expression

$$E_i = \frac{I_a}{l_0}\left(\frac{1}{1+\frac{R_1^* + R_2^*}{R_0}}\right). \quad (14)$$

In the process of experimental and technological investigations carried out at the PWI and SEC WCNE, the dependence $E_{rel} = f(k_R)$ was investigated, here the relative sensitivity E_{rel} implies the relation E_i/E_{i0}, where E_{i0} is the sensitivity at $R_1^* = R_2^* = 0$, and $k_R = 1 + (R_1^* + R_2^*)/R_0$. Moreover, it was established that the dependence $E_{rel} = f(k_R)$ has a hyperbolic character and is the most sharply expressed at $k_R < 1.2$.

In real SWS, as a rule, $k_R > 1.2$, which predetermines the possibility of rational selection of sections and weight of the wires of branches of welding circuit. Thus, for example, in the low-ampere arc welder simulator MDTS-05M1, a low-carbon steel plate (in particular, St3) is applied as SWW, whose operating length is l_0 = 360 mm, and R_0 = 0.45 mOhm. The length of the conductor of each of the branches *ac* and *bc* of the welding circuit is 0.45 m. At a 30 mm^2 cross-section of the copper conductor of each branch, the active resistance $R_1^* = R_2^*$ = 0.17 mOhm, k_R = 1.46 and (at welding current I_a = 4.5 A) E_i = 6.84 mA/mm.

The estimation of accuracy of welding speed measurement applying resistometric method, taking into account the influence of R_1^* and R_2^*, can be carried out by determining the root-mean-square error σ_{rel} according to the expression

$$\sigma_{rel} = \frac{dV_w^*}{V_w} = \sqrt{\left(\frac{dl_0}{l_0}\right)^2 + \left(\frac{dR_1^*}{R_0 + R_1^* + R_2^*}\right)^2 + \left(\frac{R_1^* + R_2^*}{R_0 + R_1^* + R_2^*}\right)^2 + \left(\frac{dR_0}{R_0}\right)^2 + \left(\frac{dI_a^*}{I_a}\right) + \left(\frac{di}{i}\right)^2}, \quad (15)$$

where dV_w^* is the differential of the function V_w^*; $i = dI_1^*/dt$ or $i = dI_2^*/dt$; $di = d(dI_1^*\,dt)$ or $di = d(dI_2^*/dt)$.

Since in the expression (15) the summands, containing R_0, R_1^*, R_2^*, as is shown by numerical analysis, are negligibly low, then the formula for determining σ_{rel}, can be represented with a sufficiently accurate approximation, in the form as:

$$\sigma_{rel} = \sqrt{\left(\frac{dl_0}{l_0}\right)^2 + \left(\frac{d(I_1^* + I_2^*)}{I_1^* + I_2^*}\right)^2 + \left(\frac{di}{i}\right)^2}. \quad (16)$$

The expression (16) allows making the conclusion that the error of measurement V_w is determined by the errors in the measurements of l_0, I_1^*, I_2^*, dI_1^*/dt or dI_2^*/dt, which, in their turn, depend on accurate characteristics of respective tools and measuring devices.

The resistometric method can be realized using analog or digital WSCD.

To the advantages of analog WSCD the comparative simplicity of circuit solutions and algorithms for their operation, high quick response, possibility of using an elementary base of mass application, relatively low cost should be attributed, and among the drawbacks: the limited accuracy of differentiating signals reflecting changes in the arc spot coordinate and the need in periodic readjustments to compensate the drift of zero values of output signals of operational ampli-

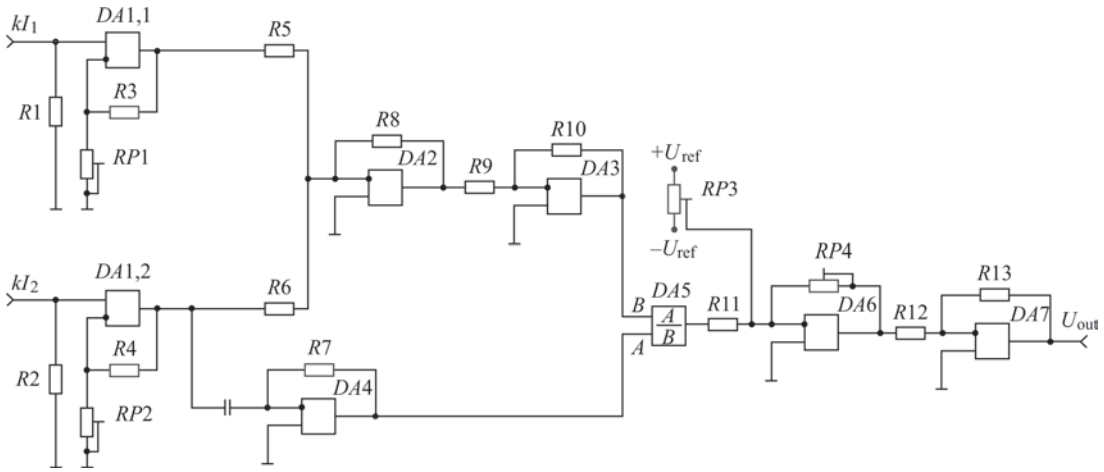

Figure 3. Simplified elementary electric diagram of one of the variants of plotting analogue WSCD

fiers and instrumental recalibrations when changing the initial conditions (SWW dimensions, arc current values I_a, etc.) should be mentioned.

Figure 3 shows a simplified electrical diagram of one of the possible variants for plotting the analog WSCD. The device contains input scaling amplifier *DA*1, adder *DA*2, which also performs the scaling function, functional divider *DA*5, inverting amplifier *DA*3, differentiating amplifier *DA*4 and realizing the function $U_{out} = k(AU_{in})$, where k and A are proportionality and scaling factors, respectively, output amplifiers *DA*6 and *DA*7. The setting-up resistors *RP*1 and *RP*2 serve for readjusting the device, and the resistors *RP*3 and *RP*4 serve for its calibration. The levels of output signals of the device displaying the arc spot coordinate x^* and welding speed V_w^* are selected based on the required range of standard signals, for example, ± (0–5) V or ± (0–10) V.

As compared to analogue ones, the digital WSCD provide a significantly higher interference immunity and measurement accuracy, possibility of in-process changing in operation and performance of calibrations and readjustments, stability of parameters in the acceptable range of changes of influencing climatic factors of the outer environment using the algorithm programming means. Moreover, as the digital WSCD include such a functional unit as an analog-to-digital converter (ADC), which is complicated as to its internal structure and a relatively expensive one, the cost of digital WSCD significantly exceeds the cost of analog devices.

The block diagram of the variant of a digital WSCD is shown in Figure 4. The device is composed of normalizing amplifiers *DA*1.1, *DA*1.2 and ADC *DA*4. To improve the interference immunity of ADC, the active low-pass filters with a single amplifying by *DA*2 and *DA*3 are introduced into the device. The normalizing amplifiers *DA*1.1 and *DA*1.2 provide the input of signals in the regulated range of levels, for example, ± (0–1.25) V or ± (0–2.5) V to the analog inputs of ADC. The type of ADC is selected from the conditions of its compatibility with a personal computer (PC), including the levels of output signals of ADC and software. At the same time, it should be noted that since almost every ADC, intended for input of information into PC, has at least eight analog input channels, it can be used not only to enter the information about the arc spot coordinate and welding speed, but also about the voltage (length) of the arc, angular positions of electrode of the welding tool simulator and other parameters characterizing the process of training or testing.

Both analogue and digital WSCD should provide their calibration, taking into account the initial conditions: geometrical dimensions of SWW, active resistances of wires and transient resistances of contact connections of branches of welding circuit, influence of factor k_R, sensitivity E_i. The calibration of analog WSCD is more labor-consuming and requires the use

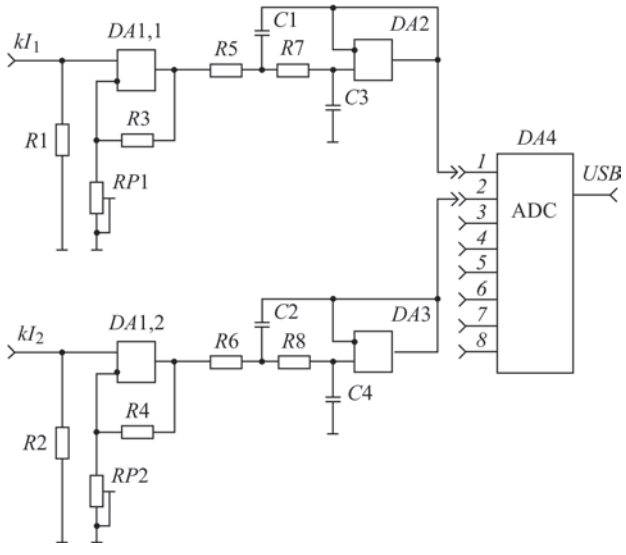

Figure 4. Simplified electric principal circuit of one of the variants of digital WSCD construction

of additional measuring equipment, for calibration of digital WSCD it is enough to have the software means.

The obligatory sensor components of both analog and digital WSCDs are two identical current sensors, which should have a linear transmission characteristic (nonlinearity coefficient of ≤ 0.5 %) in the whole range of possible changes of welding current, independently of its shape and polarity, high accuracy (the given error is not more than ± 1 %), wide dynamic and frequency range (transmission band of not less than 50 kHz), resistance to effect of inductions and interferences, always occurring during arc welding. In addition, the sensors should provide galvanic isolation of input and output circuits and should not introduce the significant additional resistances into the welding circuit. As-applied to arc SWS, the sensors based on the Hall effect the best comply with these requirements, including current sensors serially produced by a number of companies, including LEM (Switzerland) and OJSC «LEM Rossia» (RF), for example, the current sensors LAH25-NP with current measurement error of ± 0.3 %, PJSC «CHEZARA» (Ukraine), for example, the current sensors DIT-50M, DST-250, DST-500 with the measurement error of ± 0.1 %. Such current sensors have a potential or current output. The latter allows forming a link between the information output of the sensor and the WSCD input amplifier in the form of a «current loop», and thus, significantly improving the interference immunity of the device, but in this case the input stages of WSCD should be performed using the «current-voltage» converter scheme.

At the PWI together with SEC WCNE the experiments were carried out for checking the accuracy of digital WSCD, included into the computerized low-ampere arc welder simulator MDTS-05M1 and the arc welder simulator TSDS-06M. For movement of non-consumable electrode along the fixed SWW at the preset speed, the installation mechanism was used, assembled on the base of the automatic machine ADSV-6 for argon-arc welding. The source for arc supply in the case of MDTS-05M1 was the welding power module MSS-05 of this simulator, operating in the mode of a current source and providing welding current (4.5 ± 0.3) A throughout the whole technologically grounded range of the arc length, and in the case of TSDS-06M the power module based on the universal welding inverter «PROFI TIG 200», operating also in the mode of current source and providing the welding current of 80, 100, 120, 140, 160 and 180 A with the accuracy of ± 5 was used. As the SWW, in case of using MDTS-05M1 a plate of St3 was used, the total length of which was 440 mm (working length l_0 = 360 mm), width 40 mm, thickness 2 mm, and in case of using TSDS-06M a plate of the same steel, the total length of which was 470 mm (working length l_0 = 390 mm), width 60 mm, thickness 10 mm was used. The welding was performed at a constant speed of movement of non-consumable electrode (rated diameter was 2.0 mm in case of MDTS-05M1 and 3.0 mm in case of TSDS-06M) of 2, 5 and 8 mm/s, at each fixed value of welding speed, after each pass (of 360 and 390 mm length, respectively), the arc passing was performed in the opposite direction. Each experiment was repeated at least five times. The values of welding speed obtained with the help of the system WSCD — PC of the simulators MDTS-05M1 and TSDS-06M, were compared with the values of the speed of electrode movement, controlled by the devices (in particular, by ammeters of M42100 type) of the experimental installation mentioned above at the error, not exceeding ± 1.5 %. It was established by the statistical processing of experiments results that the relative error in measuring welding speed with the help of digital WSCD in case of MDTS-05M1 did not exceed ± 2.0 %, and in case of TSDS-06M ± 2.5 %.

It should be emphasized that resistometric method for determining the linear coordinate of welding arc spot and measuring welding speed, as well as digital WSCDs for its realization, were successfully applied in the hardware-software simulating complexes (welding simulators) MDTS-05M1, TSDS-06M and TSDS-06M1, designed at the PWI together with SEC WCNE [14–17]. They are widely represented and operate in Ukraine and in a number of countries of near and far abroad (for example, in Kazakhstan, Belarus, RF, Macedonia, China and other countries). Only in Russia, more than 1200 such hardware-software simulating complexes are in operation. Moreover, in a number of their educational institutions, training and certification centers, the whole simulating classes and laboratories were created on the base of these simulators to train operators in MAW, TIG and MIG/MAG welding. The experience in applying these means of technical training confirms their high operation reliability, economical efficiency and effectiveness both in the professional selection and in the initial professional training of welders, as well as for improvement of welding personnel skills, industrial training and testing, and in some cases for admittance control.

Conclusions

1. Resistometric method of measuring welding speed provides the possibility of determining linear coordinate of welding arc spot and speed of its movement in arc SWS applying a comparatively simple method with acceptable validity.

2. Taking into account the trends of development of SWS, the most challenging devices providing realization of resistometric method for determining linear coordinate of welding arc spot and measuring welding speed are digital WSCD.

3. In some cases, the resistometric method of measuring welding speed can also be used to solve the problems of monitoring real arc welding processes.

In conclusion, the authors consider it necessary to express gratitude to the engineers Skopyuk M.I., Gavva V. M, Cherednik A.D., Popov V.E., Muzhichenko A.F., Mukha A.A. and Oliyanenko D.S. for their valuable assistance, rendered during preparation of this work.

1. Danilyak, S.N. (1990) *Problems of construction of measuring transducers for control of welding pool heat content and welding speed for welding simulators: Simulation in training system*. Kiev, Naukova Dumka, 111–118 [in Russian].
2. Bigdash, V.D. (1990) Device for welding speed control in training welding systems. *Ibid*., 143–150 [in Russian].
3. Vasiliev, V.V., Simak, L.A., Bogdanovsky, V.A. et al. (2003) *Simulation and training systems in electric welding*. Ed. by V.V. Vasiliev. Kiev, NASU [in Russian].
4. But, S.N., Chernov, A.V., Krivin, V.V. (2003) System of movement tracking in simulator of manual arc welding operator. *Uzv. Vuzov. Elektromekhanika*, **3**, 74–75 [in Russian].
5. Rose, J.L. et al. (1984) *Closed loop control of welding process using ultrasonic measurement*. Pat. 2130369 GB, Int. Cl. G01S 15/16; B 23K99/12.
6. *Miyada Sodzaburi* et al. (1983) *Automatic measurement of welding speed by arc detection*. Pat. application 58-107273 Japan, Int. Cl. B 23K9/70.
7. Vasiliev, V.V., Danilyak, S.N., Ilchishin, A.P. et al. (1988) *Simulator for training the welding habits*. USSR author's cert. 1388935, Int. Cl. G09 B 19/24 [in Russian].
8. Vasiliev, V.V., Danilyak, S.N., Tkachenko, V.V. et al. (1991) *Simulator of welding*. USSR author's cert., Int. Cl. G09 B 19/24 [in Russian].
9. Paton, B.E., Vasiliev, V.V., Bogdanovsky, V.A. et al. (1987) *Simulator of welder*. USSR author's cert. 1302313, Int. Cl. G09 B 19/24 [in Russian].
10. Vasiliev, V.V., Danilyak, S.N. et al. (1992) *Device for control of welding speed and heat content of welding pool*. USSR author's cert. 1773622, Int. Cl. B 23K 9/10 [in Russian].
11. Lankin, Yu.N. (2001) Acoustic emission of the welding arc (Review). *The Paton Welding J*., **2**, 25–32.
12. Vasiliev, V.V., Grezdov, G.I., Simak, L.A. et al. (2002) *Modeling of dynamic systems: Aspects of monitoring and signal processing*. Ed. by V.V. Vasiliev. Kiev, NASU [in Russian].
13. Simak, L.A. (1984) Method of automatic determination of probe coordinates in conducting medium based on differential transformations. *Elektronnoe Modelirovanie*, **6**, 90–91 [in Russian].
14. Paton, B.E., Korotynsky, O.E., Bogdanovsky, V.O. et al. (2009) *Method of evaluation of parameters of welding arc movement in arc training systems*. Pat. 86609 Ukraine [in Ukrainian].
15. Lobanov, L.M., Bogdanovsky, V.O., Korotynsky, O.E. et al. (2009) *Arc simulator of welder*. Pat. 87395 Ukraine [in Ukrainian].
16. Lobanov, L.M., Bogdanovsky, V.A., Korotynsky, A.E. et al. (2009) *Simulator for training of welder of arc consumable and non-consumable electrode welding*. Pat. 2373040 RF [in Russian].
17. Paton, B.E., Korotynsky, A.E., Bogdanovsky, V.A. et al. (2010) *Method of determination of parameters of welding arc movement in training and testing of welder on arc training systems*. Pat. 2396158 C2 RF [in Russian].

Received 13.11.2017

doi.org/10.15407/tpwj2018.01.03

CALCULATION-EXPERIMENTAL INVESTIGATION OF THERMAL FIELDS IN THE PROCESS OF NONSTATIONARY SOLDERING

M.V. KULINICH[1], **V.N. BEZPALCHUK**[2], **S.G. KOSINTSEV**[1], **A.M. GUSAK**[2], **T.V. ZAPOROZHETS**[2] and **A.I. USTINOV**[1]

[1]E.O. Paton Electric Welding Institute of the NAS of Ukraine
11 Kazimir Malevich Str., 03150, Kyiv, Ukraine. E-mail: office@paton.kiev.ua
[2]Bohdan Khmelnytsky National University of Cherkassy
81 Shevchenko boulevard, 18031, Cherkassy, Ukraine

In the work theoretical and experimental methods were used to investigate temperature fields in the conditions of soldering the metal plates, contacting with a heated body. To determine thermal conditions, necessary to provide soldering (melting of solder in the joint zone), calculation of temperature distribution with time in the joint zone was carried out, depending on characteristics of «heater-plate-solder-plate» system and thermal resistance in contacts between the system elements. It is shown that by comparing the theoretically calculated and experimentally measured thermograms, it is possible to determine thermal resistance in the contact zones. On the basis of the obtained values of thermal resistance in the contacts, the modeling of thermal fields in the systems with the arbitrary dimensions of elements was carried out. 13 Ref., 7 Figures.

Keywords: *thermal fields, non-stationary process, method of finite differences, reaction soldering, permanent joint, multilayer foil, local heating*

Brazing is widely used for production of permanent joints of parts [1, 2]. This process lies in heating of parts being joined in a furnace till brazing alloy melting (stationary conditions) or local heating of a joint zone with the help, for example, of a contact with earlier heated body or under effect on it of source of concentrated heat radiation (infrared [3], laser [4] etc.) [5]. Distribution of temperature fields in the joint zone under conditions of its local heating till brazing alloy melting temperature will have non-stationary nature, since heating will be accompanied by heat removal to cold areas of the parts being joined. If there is no limitation of power of concentrated heat sources, realization of this brazing process will not cause difficulties even under conditions of repair on large-size part surface, for example, in patching a shell of material with high heat conductivity (aluminum alloys).

In the case of absence of the concentrated heat sources and large area of the joint the heaters can be used for its heating. They generate heat energy as a result of initiation of exothermal reaction in them. Powder mixtures, components of which react with heat emission, can be used as such heaters. It is known that intensity of exothermal reactions significantly increases at transfer from powder mixtures to compact materials with composite structure on their basis. Thus, works [6, 7] show that multilayer foils can be used as such composite materials. They consists of layers based on intermetallic forming elements such, for example, as Ni and Al or Ti and Al, received by PVD [8]. Initiation of self-propagating high-temperature synthesis (SHS) reaction in such systems results in heat emission intensity reaching the value of around 5–6 kW/cm^2 [9] that can provide local heating of the joint zone under intensive heat removal conditions.

Schematically such a soldering process of the same size plates can be presented as it is shown on Figure 1 (laboratory system). In such a system heater characteristics, necessary for soldering process, can be determined in experimental way, varying the mass of reaction material. However, if such an approach to determination of the heater characteristics is applicable to the plates of one size then in the case, for example, of joining the plate of small (finite) size to the plate of larger (unlimited) size will cause difficulties. Mainly, it is related with the necessity to take into account heat removal from the joint zone into the large size plate using the results received on the finite size samples. It is clear that heater parameters should be increased in order to compensate this heat removal. Still, considering that the plates are made of aluminum alloys, increase of heater mass can results in their significant overheating. This will result in a degradation of mechanical properties of the plates. From this

point of view selection of heater characteristics is the key for change of dimensions of the system elements being joined. Determination of the heater optimum characteristics, necessary for reaction soldering of the plates of random dimensions under conditions of local heating of the joint zone, could be fulfilled based on calculation of thermal fields.

At the same time, complexity of realization of this approach is caused by the fact that thermal processes in the joint zone depend on many parameters, some of them are known (for example, heat conductivity of materials being joined) or present themselves geometry and mass characteristics of the system elements, other have undetermined value, as, for example, a value of thermal resistance at contact boundary of the system elements. To eliminate this ambiguity in selection of the parameters for thermal field modelling in real systems the work proposes a method for calculation of coefficients of thermal resistance of the contacts, based on performance of comparison of experimentally measured and calculated change of temperature in finite dimension system (laboratory system). Satisfactory correspondence of the experimental and calculation data was received by means of variation of the parameters describing thermal resistance at elements' interface. This allows carrying modelling of the thermal fields under nonstationary conditions of soldering of limited size plate on the surface of unlimited size part.

Experimental and calculation methods. For description of a nonstationary process of heat distribution in 3D sample let's write down a heat conductivity equation in the following form:

$$c\rho\frac{\partial T}{\partial t} = div\left(\kappa \operatorname{grad} T\right), \qquad (1)$$

where c is the heat capacity of the material; ρ is the density; κ is the heat conductivity coefficient.

Considering that the system consists of different materials, which have different nature of heat exchange between the separate areas, it is convenient to divide it on finite elements. A finite-difference method [10, 11] is used in the work to solve this equation. It allows determining temperature values in a finite element through the values of temperatures in neighbor ones and characteristics of material heat conductivity:

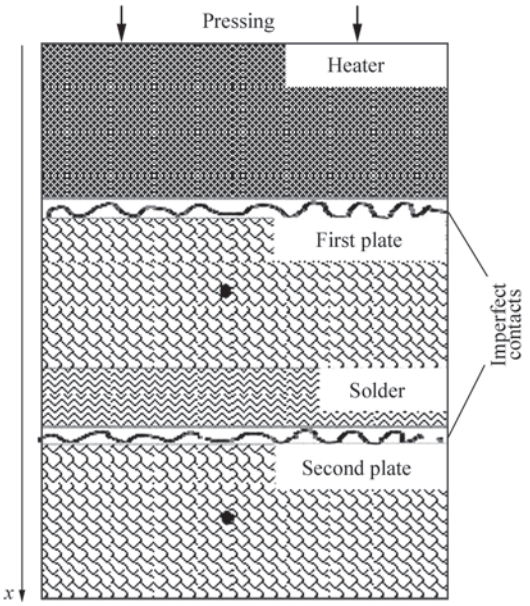

Figure 1. Scheme of obtaining the permanent joints of similar size plates (laboratory system) using soldering with the help of local heating of joint zone from external heater

$$T_{i,j,k}^{\text{new}} = T_{i,j,k} + a_k^2\left(\begin{array}{l}\dfrac{T_{i-1,j,k} - 2T_{i,j,k} + T_{i+1,j,k}}{dx^2} + \\ + \dfrac{T_{i,j-1,k} - 2T_{i,j,k} + T_{i,j+1,k}}{dy^2} + \\ + \dfrac{T_{i,j,k-1} - 2T_{i,j,k} + T_{i,j,k+1}}{dz^2}\end{array}\right) dt, \qquad (2)$$

where $a_k^2 = \kappa/(c\rho)$ is the coefficient of temperature conduction; $T_{u,j,k}$ is the temperature of finite element in point $x_{i,j,k}$.

This finite difference scheme (2) can be used for all non-boundary areas of the system. The neighbor points in boundary elements will be characterized with significantly different heat conductivities or geometry/mass parameters. Therefore, record of a density of heat flow for boundary areas is more convenient in form of temperature differences instead of temperature gradients using at that some «heat transfer coefficient» μ rather than heat conductivity κ. For example, $J = -\mu_{i,i+1}\Delta T$ for cells i and $(i + 1)$ with heat conductivity coefficients κ_i, κ_{i+1} and cell size h_i, h_{i+1}.

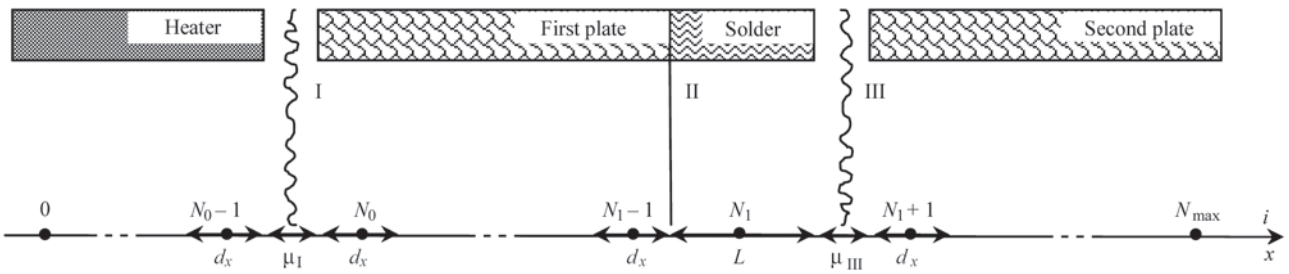

Figure 2. Scheme of division of system consisting of heater, first plate, solder and second plate on finite size plates (scheme corresponds to one-dimensional approximation)

$$\mu_{i,i+1} = \frac{2\kappa_i \kappa_{i+1}}{\kappa_i h_{i+1} + \kappa_{i+1} h_i}. \quad (3)$$

Then for cells, having neighbor cells with other coefficients of heat conductivity or size, equation (2) is changed. In one-dimensional form it is written as

$$T_i^{\text{new}} = T_i + \frac{1}{c_i \rho_i h_i}\left(-\mu_{i-1.i}\left(T_i - T_{i-1}\right) + \mu_{i.i+1}\left(T_{i+1} - T_i\right)\right)dt. \quad (4)$$

Figure 2 shows three contact zones, for which equation (4) is used:

I — between the heater and first plate (imperfect contact);

II — between the first plate and solder (ideal contact formed by means of vacuum phase deposition);

III — between the solder and the second plate (imperfect contact).

We would like to remind that imperfection of contact I means growth of thermal resistance and decrease of heat flow between the heater (cell $N_0 - 1$) and the first plate (N_0). Contact I is described by heat transfer coefficient μ_1, which in general case is uncertain quantity. Imperfection of contact III supposes thermal resistance between solder (cell N_1) and the second plate ($N_1 + 1$) (Figure 2) and is described by heat transfer coefficient μ_{III}, which is also uncertain parameter of the system. Since, as it was mentioned, contact II is an ideal, then for it the heat transfer coefficient is determined following the equation (3):

$$\mu_{N_1-1,N_1} = 2\kappa_{\text{plate1}}\kappa_{\text{solder}} / (\kappa_{\text{plate1}} L + \kappa_{\text{solder}} dx)$$

Change of the temperature from the left and right of the contact I is described by equations:

$$T^{\text{new}}_{N_0-1,j,k} = T_{N_0-1,j,k} + \left(\begin{array}{l} -\dfrac{a^2_{\text{heater}}}{dx^2}(T_{N_0-1,j,k} - T_{N_0-2,j,k}) + \\ +\dfrac{\mu_1 a^2_{\text{heater}}}{\kappa_{\text{heater}} dx}\left(T_{N_0,j,k} - T_{N_0-1,j,k}\right) \end{array}\right) dt,$$

$$T^{\text{new}}_{N_0,j,k} = T_{N_0,j,k} + \left(\begin{array}{l} -\dfrac{\mu_I a^2_{\text{plate1}}}{\kappa_{\text{plate1}} dx}(T_{N_0,j,k} - T_{N_0-1,j,k}) + \\ +\dfrac{a^2_{plate1}}{dx^2}\left(T_{N_0+1,j,k} - T_{N_0,j,k}\right) \end{array}\right) dt. \quad (5)$$

Contacts II and III refer to the solder, which is in solid state at low temperatures $T < T_{\text{out}}$, liquid at $T > T_{\text{out}}$ and preserve constant temperature T_{out} at rising portion of liquid phase η in process of melting. Therefore, it is convenient to enter temporary variables T_{XL}, T_{XR} for the left and right boundary of the solder. Using a condition of continuity of the heat flows the following can be found in these boundaries:

$$T_{XL} = \frac{(\kappa_{\text{solder}} dx T_{N_1,j,k} + L\kappa_{\text{plate1}} T_{N_1-1,j,k})}{L\kappa_{\text{plate1}} + \kappa_{\text{solder}} dx},$$

$$T_{XR} = \frac{(L\mu_{III} T_{N_1+1,j,k} + 2\kappa_{\text{solder}} T_{N_1,j,k})}{2\kappa_{\text{solder}} + L\mu_{III}}. \quad (6)$$

Then the heat flows to solder and from it:

$$J_{\text{in}} = -2\kappa_{\text{plate1}}\kappa_{\text{solder}} \frac{(T_{N_1,j,k} - T_{N_1-1,j,k})}{L\kappa_{\text{plate1}} + \kappa_{\text{solder}} dx},$$

$$J_{\text{out}} = -\frac{\mu_{III} \dfrac{2\kappa_{\text{solder}}}{L}}{\mu_{III} + \dfrac{2\kappa_{\text{solder}}}{L}}(T_{N_1+1,j,k} - T_{N_1,j,k}), \quad (7)$$

where J_{in}, J_{out} are the input and output heat flows for solder cell (we describe it using only one cell, which at low temperatures correspond to solid state, at high to liquid ones, and in intermediate period to double phase system solid body-liquid with eutectic temperature).

When solder temperature is lower than the eutectic temperature (solid solder) or higher (liquid), it is determined by equation

$$T^{\text{new}}_{N_1,j,k} = T_{N_1,j,k} + (J_{\text{in}} - J_{\text{out}})dt / c_{\text{solder}}\rho_{\text{solder}} dx. \quad (8)$$

Then the heat flow into the solder as well as from it will be described in the following way:

$$\eta^{\text{new}} = \eta + (J_{\text{in}} - J_{\text{out}})dt / \lambda L \rho_{\text{solder}}, \quad (9)$$

where L, λ, ρ are the thickness of solder layer, specific heat of melting and density, respectively.

Solder heat conductivity coefficient κ_{solder} varies as $\kappa_{\text{solder}} = \kappa^{\text{liquid}}_{\text{solder}}\eta + \kappa^{\text{solid}}_{\text{solder}}(1-\eta)$ in accordance with change of content of liquid and solid phase. Moreover, we suppose that after complete melting of solder thermal resistance between it and the second plate is significantly reduced (i.e. heat transfer coefficient $\mu^{\text{new}}_{\text{III}}$ rises) due to increase of area of a contact surface of liquid solder with a surface of the second plate. Taking this in account, change of μ_{III} coefficient after melting beginning can be presented in form of

$$\mu^{\text{new}}_{\text{III}} = \kappa_{\text{plate 2}} \times$$
$$\times\left(\mu_{\text{solid}}(1-\eta) + \eta\frac{2\kappa^{\text{liquid}}_{\text{solder}}}{L}\right) / \left(\kappa_{\text{plate 2}} + \frac{\eta\kappa^{\text{liquid}}_{\text{solder}} dx}{L}\right), \quad (10)$$

where μ_{solid} is the coefficient of heat transfer between solid phase of solder and second plate. In a limiting case $\eta = 0$ equation (10) comes to $\mu^{\text{new}}_{\text{III}} = \mu_{\text{solid}}$. In the other limiting case it is simplified into

$$\mu^{\text{new}}_{\text{III}} = \frac{2\kappa_{\text{plate 2}}\kappa^{\text{liquid}}_{\text{solder}}}{L\kappa_{\text{plate 2}} + \kappa^{\text{liquid}}_{\text{solder}} dx},$$

i.e. matches with the general equation (3). As a consequence, equation (3) can be written for the final boundary cells of the system, if consider that existence of imperfect contacts between the different elements leads to appearance of thermal resistance, and solder melting takes place at some temperature. This approach is described in more details in work [12]. Its application allows calculating temperature distribution at each moment of time depending on system parameters and in such a way trace change of temperature in a set point of the system.

It is necessary to compare calculated values of temperature with experimentally measured for checking this approach used in description of the thermal fields in a nonstationary soldering mode. A system consisting of a heater and two plates of AMg6 alloy of 5 mm thickness and 50×50 mm size, divided by solder (eutectic alloy Al–Si) layer (100 μm) deposited on the first plate, was investigated for this purpose. A multilayer Al/Ni foil was used as a heater. It was located over the first plate and pressed with set force (about 1000 N). After that SHS reaction accompanied by intensive heat emission was initiated in a nanofoil using current pulse. Redistribution of heat from the heater to the plates resulted in system heating to necessary temperature. Temperature was measured using two thin thermal couples established in the plate center (Figure 1). The thermocouples were connected to computer by ADC with sampling frequency 1 kHz. Received data were used to determine model parameters.

Results and discussion. Calculations of thermal fields of the system were carried out to determine solder melting conditions. They were based on characteristics of used materials and their thickness, at variation of heater thickness d_n. Figure 3 presents the calculated variations of the temperature in the first plate, received taking into account an assumption that rate of SHS reaction in the heater is significantly larger than heat distribution. This assumption is based on the fact that time of «burning» of 5 mm thick foil makes 0.05 s [13] at 100 cm/s rate of front distribution in SHS reaction. In this case characterization of the heater was grounded on its geometry and temperature, which it reaches as a result of SHS reaction. The time of its heating to maximum temperature was neglected at that. It can be seen that increase of heater thickness promoted rise of the maximum heating temperature of the first plate and all system in whole (the calculations were carried out in adiabatic conditions). If solder melting temperature is set then the system can be heated to necessary level by increase of heater thickness d_n. For example, 3 mm thick heater provides melting of solder with 700 K melting temperature (Figure 3) that effects the dependence of temperature in the center of first plate on time of contact with heater (calculation data) in form of «shelf». It should be noted that temperature of the «shelf» is somewhat higher than temperature of solder melting, moreover, this difference rises at increase of heater thickness (its heating value) as a consequence of temperature gradient present in the first plate, which is increased normal to heating rate.

It can be supposed that the heating rate of the first plate will significantly depend on thermal resistance of the contact between the heater and the first plate. Figure 4 presents calculation data at similar thickness

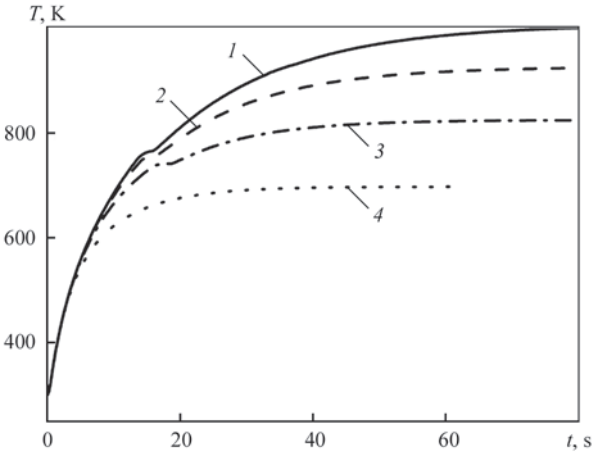

Figure 3. Effect of heater thickness on kinetics of temperature change in the center of first plate: *1* — d_n = 5 mm; *2* — 4; *3* — 3; *4* — 2

of heater (3 mm), but with different value of thermal resistance in the contact between the heater and the first plate. It can be seen that change of the thermal resistance value significantly varies heating rate that is reflected in solder melting time, i.e. time till complete melting of solder rises from 5 to 30 s at thermal resistance increase by order.

Since solder temperature and level of its melting are the result of heat balance between a heat flow from the heater into the first plate and heat flow from the solder into the second plate, it can be supposed that thermal resistance at the interface between the solder and the second plate will also effect the change of solder temperature. In fact, as can be seen from Figure 5, rise of heat conductivity in the contact zone between the solder and the second plate leads to delay of heating of the first plate, and, respectively, solder. However, regardless the fact that decrease of heat conductivity at the boundary between the solder and the second

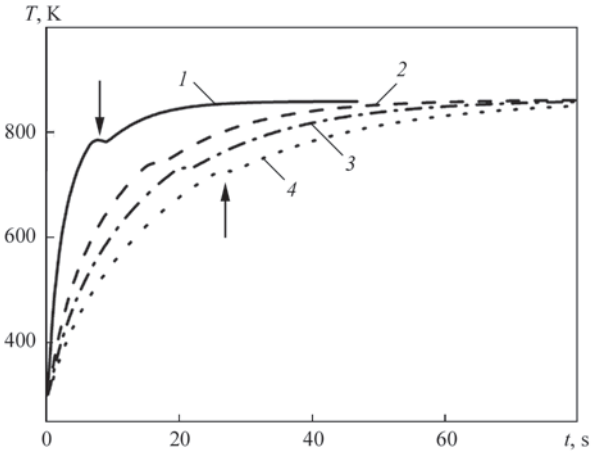

Figure 4. Dependence of temperature of first plate on time at different characteristics of heat resistance at heater – first plate interface: *1* — $\mu_0 = 5 \cdot 10^4$ W(m^2·K); *2* — $1 \cdot 10^4$; *3* — $7 \cdot 10^4$; *4* — $5 \cdot 10^3$. Characteristics of heat conductivity of solder and second plate contact are constant (arrows indicate peculiarities of temperature change promoted by solder melting (its completion))

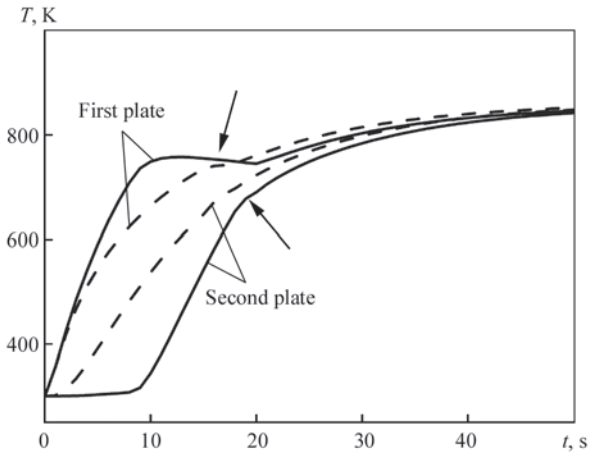

Figure 5. Dependence of temperature in the middle of plates on time at different characteristics of heat resistance at solder — second plate interface: $\mu_1 = 5 \cdot 10^2$ (*solid line*); $5 \cdot 10^4$ W/(m^2·K) (*dashed*). Characteristics of heat conductivity of contact of heater and first plate are constant (designation of arrows is the same as in Figure 4)

plate results in earlier solder melting, time till its end rises. It can be observed from temperature to time dependence in a middle of the second plate (Figure 5) that solder melting is finished when its temperature reaches solder melting temperature.

Proceeding from the fact that soldering process takes place under condition of complete melting of solder, the results of calculations indicate that the value of heat conductivity of the contact between the solder and the second plate does not have significant effect on time of this process completion.

Figure 6 presents the calculation and experimental data in the system described above, measured with the help of thermal couples, fixed in the middle of first and second plates. It can be seen that temperature of the first plate, contacting with the heater dramatically rises from the moment of SHS reaction start in the heater. However, in 8–9 s heating rate of the first plate

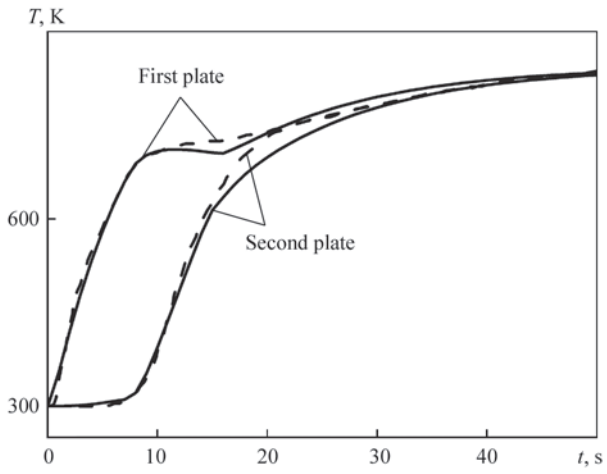

Figure 6. Experimentally measured (*dashed line*) and calculation (*solid line*) temperature in the middle of first and second plates in soldering at their local heating with the help of heater being in contact with first plate

dramatically changes. During this time temperature of the first plate and attached to it solder reaches solder melting temperature (around 700 K). Based on this it can be supposed that a delay of temperature growth in the first plate is caused by solder melting.

In favor of this is the evidence of a point of start of temperature increase in the second plate. Such a delay in heating time of the second plate can be explained by high thermal resistance in the contact between solder and second plate. After solder melting a heat contact between it and the second plate is improved that promotes redistribution of heat from solder to the second plate and its heating to the temperature level of the first plate.

Change of temperature in the system in process of its heating, qualitatively similar to that is observed experimentally (Figure 6), was calculated by means of variation of parameters of heat resistance in the contacts. At that it was supposed that heat resistance at the interface between the solder and the second plate will disappear in the moment of solder melting.

Based on this it was assumed that the calculated parameters of heat resistance in the contacts under these conditions of soldering process can be used for calculation of temperature fields in the case when the first plate is connected to the second plate, size of which is significantly larger, i.e. for 3D case.

Figure 7 represents the temperature distribution in a cross-section of the system, consisting of heater, first plate with deposited solder and second plate of larger size in the moment when solder temperature reaches the temperature of its melting (condition necessary for soldering). It can be seen that heat exchange between the system elements results in heat distribution from the heater to the first plate and then through the solder to the second plate. In contrast to laboratory assembly in this case heat is distributed along the second plate outside the dimensions of the first plate. However, as can be seen from Figure 7, such a «spread» of heat in a volume of the second plate is not critical from point of view of achievement of temperature conditions for soldering in the contact between the first and second

Figure 7. Distribution of temperature in cross-section of system (1/4 of its part is shown) at its local heating in the moment of solder melting. Length and width of second plate 3 times exceed length and width of first plate

plates. The calculations showed that only 10–20 % increase of heater thickness is enough to compensate these heat losses in the case of joining the plates of equal thickness.

Conclusions

1. The calculation of thermal fields in soldering under nonstationary heating conditions with the help of local heat source of limited energy capacity showed that there is principal possibility to achieve melting of solder in form of thin interlayer between two plates with high heat conductivity.

2. It is shown that under adiabatic conditions the soldering time, necessary for melting of solder between the plates, significantly depends on parameters of heat contact between the heater and the first plate, but almost does not depend on parameters of heat contact between the solder and the second plate.

3. Their values can be determined based on experimentally measured thermograms for laboratory system, consisting of the elements with similar contact areas by means of self-consistent calculation including variation of parameters, characterizing heat resistance in the contacts.

4. Obtained parameters of heat resistance can be used in modelling of thermal fields in the systems for soldering of parts with random dimensions. It is shown that 10–20 % increase of energy capacity and, thus, thickness of heater, is necessary to achieve solder melting at transfer from laboratory to «real» system with «endless» second plate.

1. Merzhanov, A.G., Borovinskaya, I.P. (1972) Self-propagating high-temperature synthesis of refractory inorganic compounds. *Dokl. Akad. Nauk SSSR*, **204**, 366–369 [in Russian].
2. Sytschev, A.E., Vadchenko, S.G., Boyarchenko, O.D. et al. (2013) SHS welding by thermal explosion: Ti–Ti and Ti–NiAl joints. *Int. J. of Self-Propagating High-Temperature Synthesis*, 22(**2**), 99–102.
3. Ren-Kae Shiue, Chen Chia-Pin, Wu Shyi-Kaan (2015) Infrared brazing of Ti50Ni50 shape memory alloy and 316L stainless steel with two silver-based fillers. *Metallurg. and Mater. Transact. A*, 46(**6**), 2364–2371.
4. Nothdurft, S., Springer, A., Kaierle, S. et al. (2016) Stonis-Laser soldering and brazing of steel-aluminum sheets for tailored hybrid tubes. *J. of Laser Applications*, 28, **2**, https:doi.org/10.2351/1.4943996.
5. Jacobson, D.M., Humpston, G. (2005) *Principles of brazing*. USA.
6. Morsi, K. (2001) Review: Reaction synthesis processing of Ni–Al intermetallic materials. *Mater. Sci. & Engin. A*, 299(**1–2**), 1–5.
7. Weihs, T., Barmak, K., Coffey, K. (2014) Fabrication and characterization of reactive multilayer films and foils. *Metallic Films for Electronic, Optical and Magnetic Applications: Structure, Processing and Properties*, **40**, 160–243.
8. Ustinov, A.I., Olikhovska, L.O., Melnichenko, T.V., Shyshkin, A.E. (2008) Effect of overall composition on thermally induced solid-state transformations in thick EB PVD Al/Ni multilayers. *Sur. and Coat. Tech*., **202**, 3832–3838.
9. Kravchuk, M.V., Ustinov, A.I. (2015) Influence of thermodynamic and structural parameters of multilayer foils on SHS process characteristics. *The Paton Welding J*., **8**, 8–13.
10. Farlow, S. (1985) *Partial differential equations for scientists and engineers*. Moscow, Mir [in Russian].
11. Tikhonov, A.N., Samarsky, A.A. (1977) *Equations of mathematical physics*. Moscow, Nauka [in Russian].
12. Bezpalchuk, V.M., Zaporozhets, T.V., Kravchuk, M.V. et al. (2015) Calculation of thermal fields in multiphase 3D system under nonstationary conditions of its heating. *Visnyk ChNU*, 349(**16**), 38–49 [in Ukrainian].
13. Zaporozhets, T.V., Gusak, A.M., Ustinov, A.I. (2010) SHS reactions in nanosized multilayers – analytic model versus numeric model. *Int. J. of Self-Propagating High-Temperature Synthesis*, 19(**4**), 227–236.

Received 27.11.2017

doi.org/10.15407/tpwj2018.01.04

STRESS-STRAIN STATE OF WELDED JOINTS FROM ALUMINIUM ALLOYS UNDER THE CONDITIONS SIMULATING OPEN SPACE*

E.A. ASNIS, E.G. TERNOVOJ, E.A. VELIKOIVANENKO, A.S. MILENIN and **G.F. ROZYNKA**
E.O. Paton Electric Welding Institute of the NAS of Ukraine
11 Kazimir Malevich Str., 03150, Kyiv, Ukraine. E-mail: office@paton.kiev.ua

The paper gives the results of computational research of the influence of light-shade boundaries promoting preheating of joints of sunlit plates to be welded and their intensive cooling on the shaded side during electron beam welding under the conditions simulating open space, on the stress-strain state. A set of numerical procedures and software for computer modeling of the kinetics of temperature fields, stresses and strains in butt fusion welding of plates from aluminium alloy AMg6, allowing for essentially non-uniform external temperature impact were developed for this purpose. The influence of the position of light-shade boundaries relative to the weld on the forming instantaneous and residual stressed state of aluminium plates in welding was analyzed. For this purpose the respective problems of nonstationary thermoplasticity were solved by finite element method, based on computational temperature field kinetics, determined allowing for the features of the impact of welding heat source and conditions of external heating and cooling. Performed calculations showed, in particular, that distribution of residual stresses forming in welded joints of plates from aluminium alloy AMg6 at different position of light-shade boundaries, is characterized by maximum stresses, which do not reach the base metal yield limit (170–180 MPa). Such stresses should not essentially lower the mechanical characteristics and performance of welded parts and components, produced in open space conditions. 6 Ref., 3 Figures.

Keywords: *simulation of open space conditions, light-shade boundary, stressed state, mathematical modeling*

Performance of welding operations in open space can often be a necessary technological procedure in mounting and repair-reconditioning operations for critical structural elements of space vehicles in long-term operation. Selection of specific welding parameters, which guarantee the joint quality, is connected with allowing for the peculiarities of the influence of space factors (low gravity, deep vacuum, frequent change of light-shade boundaries, etc.) [1, 2]. One of the main features of welding in open space are extreme temperature variations between the shaded and illuminated part of the structure: in the sunlit section of the orbit the surface of space vehicle elements can heat up to the temperature of 120 °C, and sometimes even higher, whereas in the shaded areas the temperature drops to –100 – –120 °C [1].

Nonuniform external temperature field influences not only the welding process proper, in view of the different heat input depending on the position of light-shade boundary, but also formation of weld metal and heat-affected zone (HAZ) under the conditions of different preheating and cooling, as well as the features of structure thermal deformation.

Aluminium alloys are the main structural materials for space vehicle construction. At structure preheating up to 100–120 °C prior to welding, weld pool dimensions increase and liquid metal overcooling on the solidification front is reduced that leads to increase of the crystallite size and promotes lowering of weld strength [3]. On the shaded side metal resistance to solidification crack formation can decrease, because of low temperatures, although lowering of initial temperature has practically no influence on weld metal mechanical properties [4]. Arising stresses in welded joints can further influence lowering of hot cracking resistance of weld metal and can lead to deterioration of structure performance that is particularly important at long-term operation of space vehicles.

In view of a quite limited number of welded samples, produced in open space and delivered to Earth [1], no investigations of their stress-strain state (SSS) were conducted. As experimental evaluation of the influence of open space conditions on welded joint SSS involves objective difficulties, application of mathematical and computer modeling methods is the rational approach.

*Participated in work performance S.A. Glushak, T.A. Likarenko.

The objective of this study consisted in numerical analysis of peculiarities of SSS in a butt welded joint produced under the conditions simulating open space, at different position of light-shade boundary.

A set of mathematical models and tools for their computer implementation was developed, which allow solving joint tasks of temperature field kinetics under the impact of a rapidly moving welding heat source, and spatially nonuniform field of ambient temperatures. Development of stresses and strains was assessed in butt welded plates (plane stressed state, Figure 1). Solved for this purpose was the problem of nonstationary heat conductivity for temperature field $T(x, y)$ under the impact of a welding heat source of power W:

$$\frac{\partial}{\partial x}\left(\lambda(T)\frac{\partial T(x,y)}{\partial x}\right)+\frac{\partial}{\partial y}\left(\lambda(T)\frac{\partial T(x,y)}{\partial y}\right)+ +W=c\gamma(T)\frac{\partial T(x,y)}{\partial t}, \quad (1)$$

where $\lambda(T)$ is the coefficient of thermal conductivity; $c\gamma(T)$ is the bulk heat capacity; t is the current moment of time.

Proceeding from the features of surface heat removal in open space environment, boundary conditions to equation (1) were formulated as follows:

$$-\lambda(T)\frac{\partial T(x,y)}{\partial n}=\varepsilon\sigma_{SB}\left(T^4-T_C^4(x)\right), \quad (2)$$

where

$$T_C(x)=\begin{cases}T_{\text{sh}}, \text{ если } x<x_0\\ T_{\text{sn}}, \text{ если } x\geq x_0\end{cases}, \quad (3)$$

where T_{sh}, T_{sn} is the ambient temperature on the shaded and sunlit sides of the structure, respectively; ε is the degree of blackness of the surface of the structure being welded; σ_{SB} is the Stephan–Boltzmann constant; x_0 is the current position of light-shade boundary; n is the normal to the surface.

Prediction of residual stresses was performed using a calculation procedure, based on consistent tracking of development of elasto-plastic deformations in points x, y on sample cross-section during heating in welding and subsequent cooling [5]. So, at any moment of time t strain tensor ε_{ij} can be represented as a sum of tensors:

$$\varepsilon_{ij}=\varepsilon_{ij}^e+\varepsilon_{ij}^p+\varepsilon_{ij}^T, \quad (4)$$

where ε_{ij}^e is the tensor of reversible elastic deformations; ε_{ij}^p is the tensor of nonelastic deformations of instant plasticity; ε_{ij}^T is the tensor of reversible temperature deformations.

Thus, we will represent incremental strain tensor $\Delta\varepsilon_{ij}$ at each tracking step as follows:

$$d\varepsilon_{ij}=d\varepsilon_{ij}^e+d\varepsilon_{ij}^p+\delta_{ij}\left(d\varepsilon_{ij}^T\right), \quad (5)$$

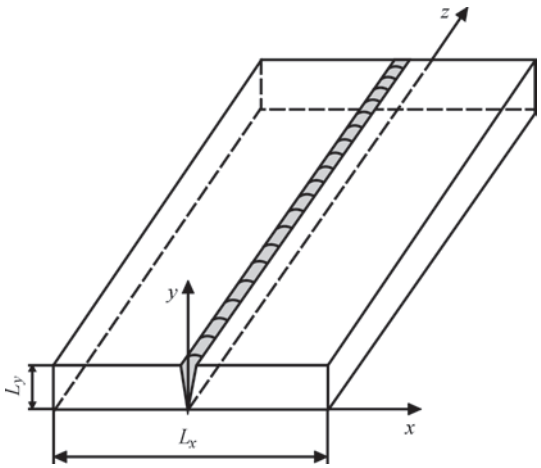

Figure 1. Schematic of sample welding

where δ_{ij} is the unit tensor or Kronecker symbol, i.e. $\delta_{ij}=1$ at $i=j$ and $\delta_{ij}=0$ at $i\neq j$.

The connection between stresses σ_{ij} and strain increments in point (x, y) at moment of time t, compared to $t = 0$, is determined by generalized Hooke's law, allowing for volume temperature and microstructural changes 3φ and associated law of plastic flow:

$$\Delta\varepsilon_{ij}=\psi\left(\sigma_{ij}-\delta_{ij}\sigma\right)+\delta_{ij}\left(K\sigma+\Delta\varepsilon_{ij}^T\right)- -\frac{1}{2G}\left(\sigma_{ij}-\delta_{ij}\sigma\right)^*-(K\sigma)^*, \quad (6)$$

where ψ is the function of the state of elasto-plastic material, determining the degree of plastic flow development; $\sigma=(\sigma_{xx}+\sigma_{yy}+\sigma_{zz})/3$, $G=E/2(1+\upsilon)$ is the shear modulus; E is the modulus of normal elasticity; υ is the Poisson's ratio; $K=(1-2\upsilon)/E$ is the modulus of bulk compression.

Function ψ reflects the state of material in point x, y at moment of time t: it is either equal to $1/2G$ (elastic behaviour), or is greater than $1/2G$ (elasto-plastic behaviour). Yield condition allows constructing the iteration process of refining function ψ:

$$\psi=\frac{1}{2G}, \text{ if } \sigma_i<\sigma_s=\sigma_T(T); \quad \psi>\frac{1}{2G}, \text{ if } \sigma_i=\sigma_s; \quad \text{state } \sigma_i>\sigma_s \text{ is unacceptable}, \quad (7)$$

where σ_y is the material yield point; σ_i is the stress intensity.

Without loss of generality, a typical flat welded sample from aluminium alloy AMg6 with dimensions $L_z\times L_x\times L_y=180\times50\times2$ mm was considered for calculations, that corresponds to samples produced in space. Electron beam butt welding was performed. Welding modes were as follows: accelerating voltage U_{acc} = = 10 kV, beam current I_b = 100 mA, welding speed v_w = 8 mm/s. Depending on the position of light-shade boundary x_0 relative to welded joint line, the following welding conditions were considered:

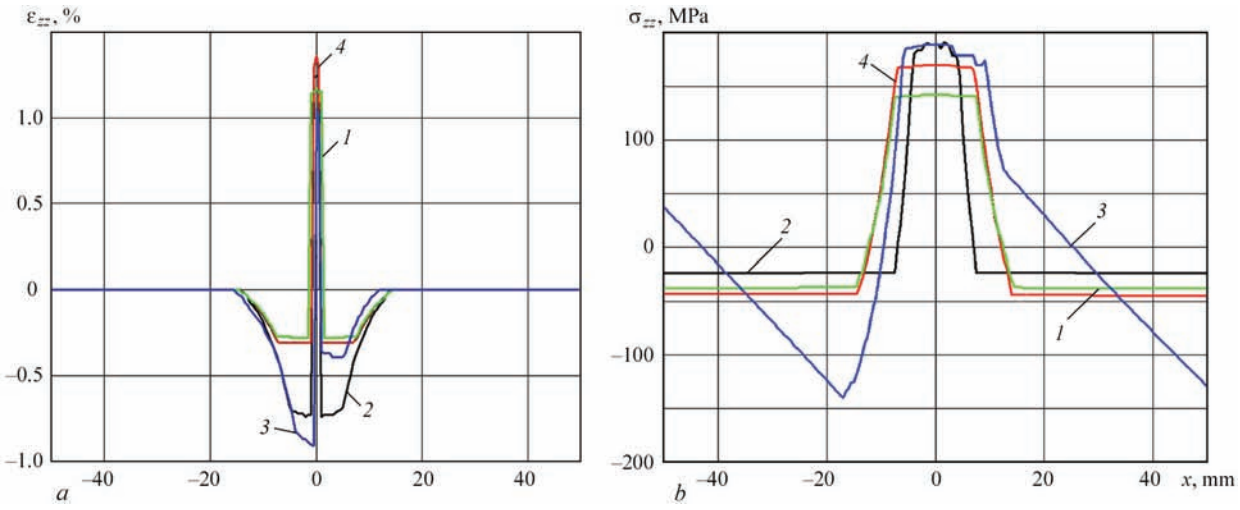

Figure 2. Distribution of residual longitudinal deformations ε_{zz} (*a*) and stresses (*b*) across the sample width at different conditions of external temperature impact: *1* — on sunlit; *2* — on shaded side; *3* — at light-shade boundary position on the butt being welded (x_0 = = 0), when one of the plates being welded is heated up to temperature T_{sn} = 120 °C (positive 0*x* half-axis), and the other is cooled to T_{sh} = –120 °C (negative 0*x* half-axis); *4* — ambient room temperature (20 °C)

1. Welding on the sunlit side ($x_0 < -L_x/2$), i.e. with preheating up to the ambient temperature $T_{amb} = T_{sn} =$ = 120 °C.

2. Welding on the shaded side ($x_0 > L_x/2$), i.e. with cooling to ambient temperature $T_{amb} = T_{sh} = -120$ °C.

3. Welding at light-shade boundary position on the butt to be welded ($x_0 = 0$), when one of the plates being welded is heated up to temperature T_{sn} = 120 °C, while the other one is cooled to T_{sh} = –120 °C.

SSS of the sample of the above dimensions after welding at room temperature (20 °C) was also calculated for comparison.

Calculations showed that transverse stresses σ_{xx} and deformations ε_{xx} have very low values, close to zero, and, that is why they are not considered further-on. Processes of irreversible deformation shrinkage in the area of local heating in welding determine formation of high longitudinal deformations ε_{zz} and stresses σ_{zz} that is characteristic for welding plates [6]. So, magnitude of deformations ε_{zz} does not exceed 1.5%, depending on temperature conditions on the boundary of the item being welded. Here, at nonuniform heating (condition 3) differences in the properties of plates being welded and heating/cooling conditions cause a slight increase of longitudinal shrinkage deformations in the structure shaded side, while total deformations remain within the generally accepted tolerances (Figure 2, *a*).

Figure 2, *b* gives the curves of residual longitudinal stresses σ_{zz}. The highest values were observed in the weld, and they practically do not differ from each other, depending on ambient temperature conditions: the differences depend on the difference in material yield points at the respective temperatures. A characteristic feature of the stress field at nonuniform heating (condition 3) are nonzero values of stresses

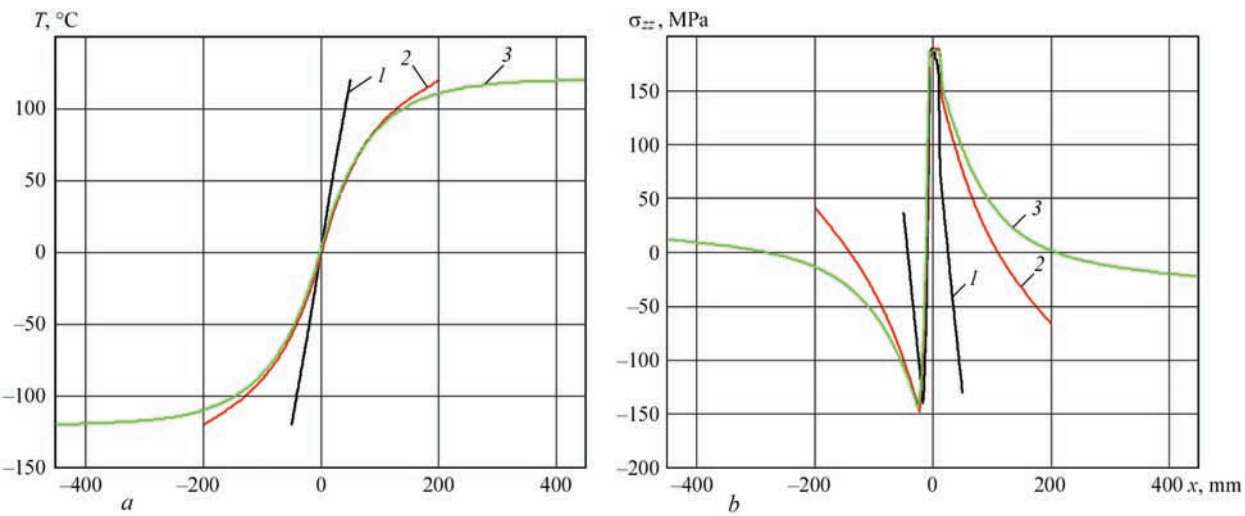

Figure 3. Influence of the width of sample being welded L_x on distribution of temperature (*a*) and longitudinal residual stresses σ_{zz} (*b*) provided the light-shade boundary is located along the weld: *1* — L_x = 100 mm; *2* — 400; *3* — 900

on sample periphery. This is associated with the fact that despite the presence of light-shade boundary on the surface of the item being welded, the temperature is distributed across the metal thickness according to metal physical properties (heat conductivity and heat capacity), so that transition from temperature T_{sh} = = –120 °C to T_{sn} = 120 °C is smooth (Figure 3, *a*). The width of the considered sample is such that the temperature gradient is preserved across its entire section, leading to formation of the respective balanced stresses. Increase of sample width neutralizes the impact of temperature gradient in the area of light-shade boundary on the stressed state on its periphery (Figure 3, *b*).

Conclusions

1. Calculation results showed that preheating and cooling do not affect the SSS of welded joints of aluminium alloy AMg6.

2. Stresses in welded joints do not exceed base material yield point. Such stresses do not have any essential influence on strength properties and performance of welded joints produced in space environment.

3. Results of numerical studies were used to demonstrate the influence of the width of butt-welded sample from aluminium alloy AMg6 on temperature and stress distribution at its nonuniform heating under the conditions simulating open space. It is shown that presence of a light-shade boundary (with temperature range from –120 °C to 120 °C) leads to formation of a transition region in the metal of about 400 mm length. Therefore, in welding smaller-sized samples stress distribution is characterized by increase of the longitudinal component relative to the item periphery.

1. Paton, B.E. (2000) *Space: technologies, materials science, structures*. Kiev, PWI [in Russian].
2. Fragomeni, J.M., Nunes Jr., A.C. (2003) A study of the effects of welding parameters on electron beam welding in the space environment. *Aerospace Sci. and Technology*, **7**, 373–384.
3. Rabkin, D.M. (1986) Metallurgy of welding of aluminium alloys. Kiev, Naukova Dumka [in Russian].
4. Bondarev, A.A., Ternovoj, E.G. (2010) Features of weld formation and properties of aluminium and magnesium alloy joints under simulated space conditions. *The Paton Welding J.*, **11**, 16–20.
5. Makhnenko, V.I. (2006) *Resource of safe operation of welded joints and assemblies of modern structures*. Kiev, Naukova Dumka [in Russian].
6. Mi, G., Li, C., Gao, Z. et al. (2014) Finite element analysis of welding residual stresses of aluminum plates under different butt joint parameters. *Engineering Review*, 34(**3**), 161–166.

Received 20.11.2017

doi.org/10.15407/tpwj2018.01.05

MANUFACTURE OF INDUSTRIAL PRODUCTS USING ELECTRON BEAM TECHNOLOGIES FOR 3D-PRINTING*

V.M. NESTERENKOV, V.A. MATVEJCHUK and **M.O. RUSYNIK**
E.O. Paton Electric Welding Institute of the NAS of Ukraine
11 Kazimir Malevich Str., 03150, Kyiv, Ukraine. E-mail: office@paton.kiev.ua

The prospects of manufacturing a wide range of parts and units of flying vehicles and engines using electron beam technologies, were noted In the work the peculiarities of developing such technology are considered using the domestic raw materials in the form of powder materials or filler wire. In the laboratory equipment the cylindrical and rectangular specimens were manufactured, thus proving the possibility of implementing the additive technology for the needs of industry. 6 Ref., 1 Table, 7 Figures.

Key words: *electron beam surfacing, products of preset shape, 3D-printing method, powder materials, filler wires, laboratory equipment*

The innovative technologies of layer-by-layer manufacture of products using the method of a rapid prototyping open up the new opportunities for manufacturing parts of a preset shape and structure with predetermined properties.

The process of manufacturing products by this method applying electron beam is relatively new, but it has already successfully demonstrated great prospects of its use in industry for manufacturing a wide range of both parts and units of flying vehicles as well as gas turbine engines. It is based on the operation of layer-by-layer fusion of metallic powder or filler wire in vacuum by electron beam. This approach is distinguished by a rapid transition to manufacture of three-dimensional products directly from the system of automated designing with the opportunity of applying a wide range of metals and alloys, including refractory and chemically active ones. All existing industrial developments for today belong to foreign companies [1]. The use of technologies and machines for prototyping in our country is associated with their purchase abroad with subsequent significant expenses for buying necessary powders [2] being a consuming and expensive component of this technology.

The aim of the present work is creating the additive technologies for manufacture of products of a preset shape and structure using the methods of layer-by-layer electron beam melting of metals in vacuum with powder materials, i.e. Electron Beam Melting (EBM), and with filler wire made in Ukraine, i.e. Direct Manufacturing (DM).

To achieve this aim it is necessary:

- to carry out investigation of properties and possibility of application of metallic powders and filler wires for realizing the additive process of manufacturing and repair of products of aerospace industry, turbine construction, machine building and medicine;
- to work out the designing documentation for basic units of 3D-printer for each of the investigating additive processes and to manufacture the experimental laboratory equipment;
- to develop software for investigations of two additive processes using electron beam (EBM and DM) [3];
- to develop additive electron beam technologies EBM and DM, and also to investigate the properties of multilayer deposited metal;
- to create an industrial mock-up of the equipment in the set with the software as-applied to the industry of Ukraine.

Topicality of work. The technologies and equipment developed will allow manufacturing metal products using the method of rapid prototyping applying the domestic raw materials.

The developing technologies and equipment are initially oriented to the needs of national enterprises. For manufacture it is supposed to use inexpensive domestic raw materials necessary for the manufacturer. This approach will also provide manufacturing parts and units by rapid prototyping, coming from the needs of a consumer and in close contact with him. The developed technologies will allow shortening the terms for implementation of new types of products, expanding

*Based on materials presented at 8th International Conference «Beam Technologies in Welding and Materials Processing», September 10–16, 2017, Odessa, Ukraine.

their range, and also creating the fundamentally new types of products with preset properties, the manufacture of which is impossible without 3D-printing methods.

Since there is no equipment for 3D-printing of national designing, it is relevant to create its hardware and software in Ukraine for realizing the additive electron beam manufacturing, free from the imported raw materials, oriented to implementation at the enterprises of aerospace industry and turbine construction: SE Research and Production Complex «Zorya»–«Mashproekt», SE «LRZ» Motor», Share-holding Company «Motor Sich» and SE «KB «Yuzhnoye».

Technology of layer-by-layer electron beam melting of metals in vacuum with application of powder materials by EBM. The technology of electron beam surfacing by EBM is similar to the selective laser melting applied in industry. Its main difference consists in using an electron gun instead of laser as a power source for melting. The technology is based on using a high-power electron beam for fusion of metallic powder in the vacuum chamber with the formation of successive layers repeating the contours of a digital model. Unlike the technology of laser sintering, the electron beam melting allows increasing the efficiency due to a high power of guns and electromagnetic, but not electromechanic, scanning of the electron beam.

As to mechanical properties, the ready products almost do not differ from cast parts. The device reads data from a file, containing a three-dimensional digital model, and deposits the successive layers of powder material. The contours of layers of the model are plotted by an electron beam, thus melting the powder at the contact areas. The melting is performed in vacuum working chambers, which allows working with chemically active metals, sensitive to oxidation, for example, with titanium and its alloys.

The electron beam melting is carried out at elevated temperatures, reaching the order of 700–1000 °C, which allows creating the parts with lower residual stresses, caused by a temperature gradient between already cooled and still hot layers. In addition, the full melting of consumable powder allows manufacturing monolithic products. Therefore, they have the maximum strength.

For development of additive technologies in Ukraine, the SE «State Research and Design Institute of Titanium» together with the Research Center «Titan of Zaporozhye» offer an innovative technology for production of low-cost titanium powders by the method of hydrogenation-dehydrogenation (HDH) from titanium sponge or other titanium-containing materials of different quality and fractional composition [4]. The use of such powders for additive manufacturing seems challenging with the availability of the appropriate equipment for 3D-printing.

Considering the abovementioned, the specialists of the E.O. Paton Electric Welding Institute started investigations in the field of developing technologies and equipment for additive manufacturing of metal products by the method of rapid prototyping applying the raw material of the SE «State Research and Design Institute of Titanium» and the Research Center «Titan of Zaporozhye». The experimental specimens of the products of the preset shape were produced and laboratory equipment for 3D-printing was designed on the basis of the installation for electron beam welding of SV-212 type. A block diagram of the equipment is shown in Figure 1.

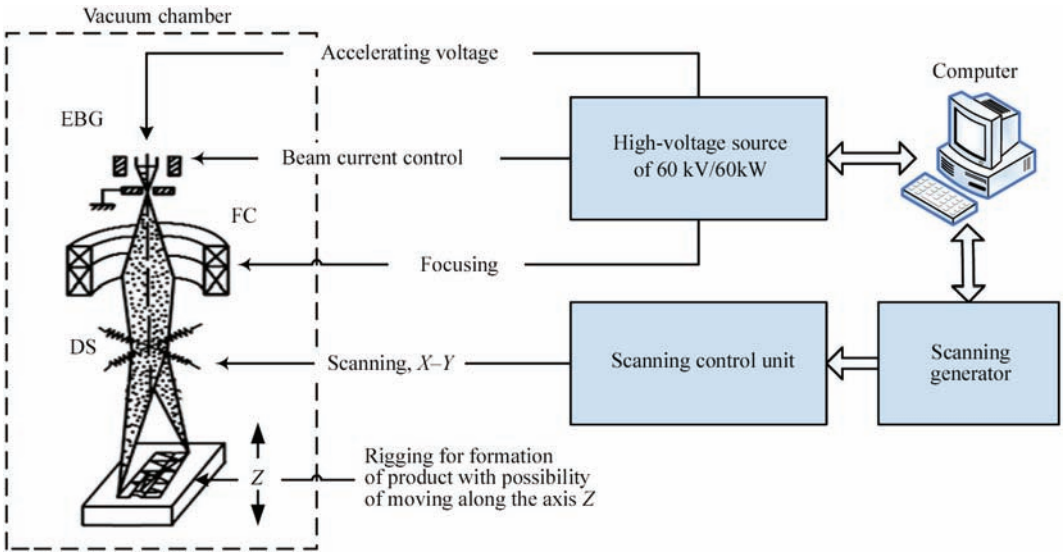

Figure 1. Block diagram of equipment for additive electron beam surfacing: EBG — electron beam gun; FC — focusing coil of EBG; DS — deflecting system of EBG

Technological characteristics and chemical composition of powder materials HDH of titanium VT1-0

Fraction, μm	Density, g/cm³	Content of impurities, wt.%					
		N	C	H	Fe	Si	O
100–160	1.7	≤0.05	≤0.1	0.01–2.00	≤0.3	≤0.15	≤0.15
63–100	1.8	≤0.05	≤0.1	0.01–2.00	≤0.3	≤0.15	≤0.15

To form melting zone, the computer-controlled scanning generator was applied. The electron beam deflects along the axes *X* and *Y* and creates the melting zone of a preset shape. The surfacing process is performed in compliance with the program according to the set technological modes. The objects of control are the beam current, focusing current, beam deflection along the axes *X* and *Y*.

The process of electron beam melting occurs in the vacuum chamber at the vacuum value being less than $1 \cdot 10^{-4}$ torr. A focused beam of electrons creates a melting zone and forms a product by moving along the preset trajectory. Then, the table in the rigging is lowered and the next layer of powder is applied. The part is layer-by-layer «grown».

As powder materials, the titanium HDH powders were used, representing granules of a non-spherical shape of the titanium alloy VT1-0.

The technological characteristics and chemical composition of HDH powder materials of titanium VT 1-0 are presented in Table.

According to the scheme mentioned above, the specimens of a rectilinear shape with the dimensions of 12×12×100 mm were produced (Figure 2). In Figure 2, the upper layer of product *1* and substrate *3* with intermediate layers of deposited metal are seen. On the lateral surface the particles of unmelted metallic powder *2* are present. This powder is further removed, and the metal surface is machined. After practicing the deposition modes, taking into account the powder fraction, the size of the layer and that of the layers overlapping, the specimens for further investigations were produced. Figure 3 shows the specimen after machining.

In different sections of the specimen, metallographic examinations of microstructure of the deposited metal were carried out (the powder from the titanium alloy VT1-0 was deposited on the base of the titanium alloy VT-20).

The structure of the deposited metal represents α-phase characteristic of the lithium titanium alloys, the defects like pores and lacks of fusion were not detected in the investigated specimens.

The designed elements of technology of layer-by-layer growing with the use of HDH powders allows manufacturing parts with a dense cast metal structure without defects [5]. The obtained results provided the basis for designing an industrial equipment for the additive manufacturing of products using powder materials.

The equipment is created on the base of the installation of type SV-212M for electron beam welding. The modernization of vacuum chamber, the development of control systems of actuators for moving the table along the vertical and the unit for powder distribution in the chamber, as well as the development of the appropriate software for reproduction of additive manufacturing are envisaged.

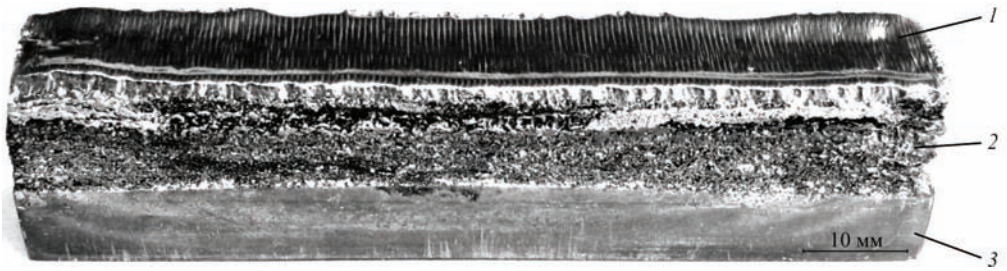

Figure 2. Specimen manufactured by electron beam 3D-deposition: *1* — upper layer of deposited metal; *2* — intermediate layer of metal with particles of unmelted powder on the sides of specimen; *3* — titanium substrate

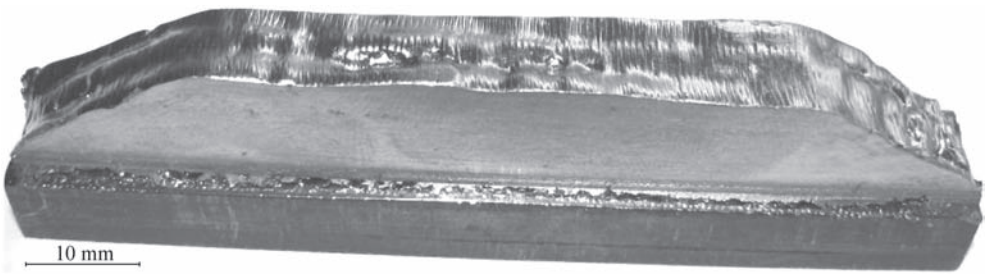

Figure 3. Appearance of specimen after machining

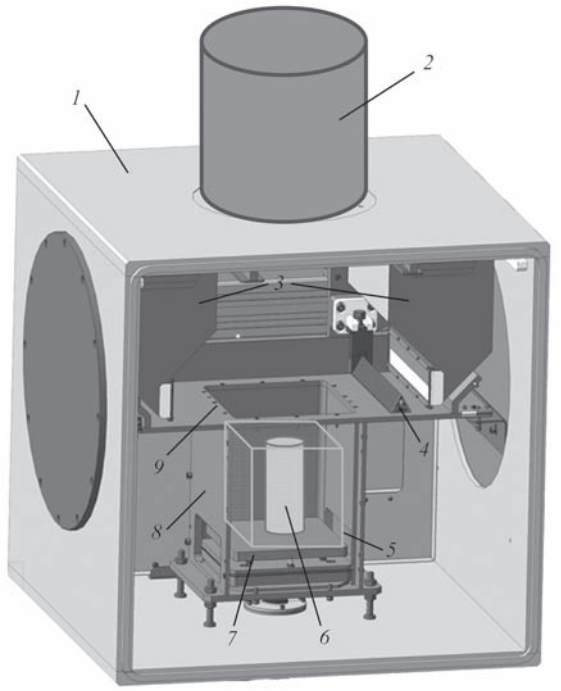

Figure 4. Scheme of installation for additive manufacturing with application of metallic powder materials (description *1–9* see in the text)

The scheme of installation is shown in Figure 4.

The process of electron beam melting occurs in the vacuum chamber *1* at the vacuum value being less than $1 \cdot 10^{-4}$ torr. The metal powder is fed in bulk to the working table *9* from the hoppers *3*. The rack *4*, moving along the table *9*, forms a layer of powder of the preset thickness on the surface of the pallet *7*. In the initial position the pallet is located at the top of the shaft *8*. The focused electron beam, formed by EBG *2*, flashes the surface of the powder along the preset trajectory. Thus, in accordance with the algorithm, the contours of a product and its layer are formed. Further, the pallet *7* is lowered to a preset value and the next layer of powder is deposited. The process is repeated. The product *6* is layer-by-layer grown. At the end of the production cycle a part is extracted from the vacuum chamber, cleaned from unmelted powder *5* and machined.

The technology of layer-by-layer electron beam melting of metals in vacuum applying powder materials allows creating dense metal products of a preset shape at the high geometric accuracy. The overall dimensions of products are 200×200×200 mm, and the efficiency of electron beam deposition according to the EBM technology does not exceed 0.3 kg of metal powder per hour.

Technology DM of layer-by-layer electron beam melting of metals in vacuum with filler wire. The second investigated DM process of electron beam melting of metals is the process of melting the metal wire in vacuum with the formation of successive layers. For heating and melting of the wire, an electron beam of the required power is used.

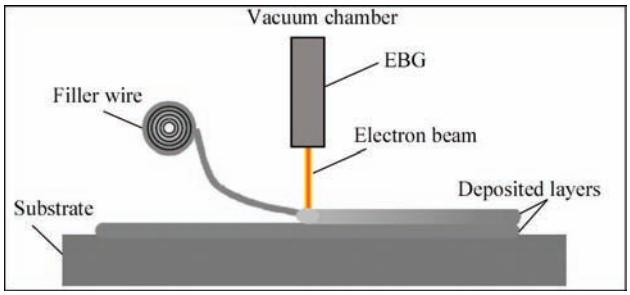

Figure 5. Scheme of layer-by-layer electron beam melting of filler wire

The scheme of DM process is shown in Figure 5.

The deposition is performed in the vacuum chamber. The filler wire is fed into the zone of electron beam effect, where it is heated and melted. The EBG and/or the substrate, on which a product is formed, are moving, forming a layer of deposited metal. The product is built by a digital model. The data of the CAD-program are converted into the CNC code. A part is layer-by-layer formed: each subsequent layer of metal is deposited on the previous one, i.e.layer-by-layer, until the product reaches the preset shape. After that, it undergoes heat and mechanical treatment.

The efficiency of electron beam melting according to DM technology varies from 3 to 9 kg of metal per hour depending on the material selected and the characteristics of a product, which makes it the fastest process of additive manufacturing [6].

The dimensions of products can vary from millimeters to several meters and are limited only by the dimensions of vacuum chamber. The DM technology allows manufacturing high-quality large-sized metal structures with more than 5 m length.

The process of electron beam melting is performed at the vacuum of less than $1 \cdot 10^{-4}$ torr, which allows working efficiently with chemically active metals like titanium, aluminium and their alloys, metals of refrac-

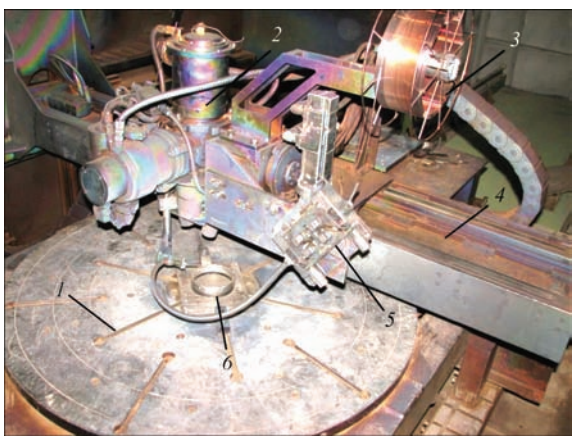

Figure 6. Location of equipment for surfacing with wire in vacuum chamber (description *1–6* see in the text)

Figure 7. Specimens manufactured according to DM technology

tory and other alloys, widely applied at the aerospace and turbine construction enterprises. The structure of products manufactured according to the DM technology is cast and defect-free.

The efficiency factor of installations for electron beam melting reaches 95 %, and the amount of wastes during machining of a final product is negligible. All this allows confirming the high efficiency and environmental cleanliness of DM additive manufacturing.

The possibility of applying filler wires of titanium alloy VT1-0, aluminium alloy ER 4043, steel welding wire Sv-08G2S and stainless steel wire ER 308 was studied.

On the base of the equipment of type KL-209 for electron beam welding, the laboratory installation for realization of DM additive process was designed. In the vacuum chamber of the installation (Figure 6) such units are located: EBG *2* of type ELA-60; multicoordinate module for movement of EBG *4*; mechanism for filler wire feeding *5* with coil *3* and rotator *1*. On the rotator the product *6* is located, manufactured according to the DM technology.

In the laboratory equipment, a satisfactory formation of round and rectangular specimens was obtained, from which it is possible to compose complex geometric shapes in the form of combination of bodies of revolution and rectangles. The wall thickness of specimens varied from 6 to 10 mm in use of four types of wires (Figure 7).

The cross-sections of all the deposited specimens are formed as a cast metal without inclusions and porosity.

As a result of carried out works, the possibility of manufacturing products of a preset shape was shown applying the methods of additive electron beam melting using domestic raw materials, which allowed proceeding with the development and manufacture of an pilot installation for realizing 3D technologies in industry.

1. Smurov, I.Yu., Kononov, S.G., Kotoban, D.V. et al. (2015) *Development of domestic additive technologies for manufacture and control of critical machine-building parts*. In: Synopsis-presentation of FGBOU VPOMGTU Stankin [in Russian].
2. Skrebtsov, A.A., Ovchinnikov, A.V., Shevchenko, V.G. et al. (2017) Producing of parts from titanium alloys by additive methods. *Stroitelstvo. Materialovedenie. Mashinostroenie. Ser.: Starodubskie Chteniya*, **95**, 118–122 [in Russian].
3. Paton, B.E., Nazarenko, O.K., Nesterenkov, V.M. et al. (2004) Computer control of electron beam welding with multi-coordinate displacements of the gun and workpiece. *The Paton Welding J.*, **5**, 2–5.
4. Zhemanyuk, P.D., Basov, Yu.F., Ovchinnikov, A.V. et al. (2016) Application of titanium powders of new generation (HDH2) in additive technologies. *Aviats.-Kosmich. Tekhnika i Tekhnologii*, 135(**8**), 139–144 [in Russian].
5. Nesterenkov, V.M., Matvejchuk, V.A., Rusynik, M.O. et al. (2017) Application of additive electron beam technologies for manufacture of parts of VT1-0 titanium alloy powders. *The Paton Welding J.*, **3**, 2–6.
6. *Electron Beam Additive Manufacturing (EBAM)*, http://www.sciaky.com/additive-manufacturing/electron-beam-additive-manufacturing-technology. 2017.

Received 28.11.2017

doi.org/10.15407/tpwj2018.01.06

ELECTRODES FOR ARC HARDFACING OF COMPOSITE ALLOYS

A.I. BELY, A.P. ZHUDRA, V.I. DZYKOVICH and **V.V. PETROV**
E.O. Paton Electric Welding Institute of the NAS of Ukraine
11 Kazimir Malevich Str., 03150, Kyiv, Ukraine. E-mail: office@paton.kiev.ua

This paper considers the peculiarities of formation of composite alloys based on tungsten carbides in arc hardfacing. It was found that application of spherical granules of tungsten carbides as a wear-resistant phase, which are to lower degree subjected to solution in process of hardfacing, is the most reasonable in development of electrode material. The optimum content of reinforcing phase in electrode metal was determined which should vary in 60–70 % limits of material weight in volume. Developed were gas-slag-forming and alloying systems and experimental compositions of the electrodes were manufactured. A series of technological peculiarities for providing coating homogeneity, consisting of components different in specific weight and granulometric composition, as well as its deposition on the electrode rod, were specified in experimental way. Determined were specifics of hardfacing process using developed electrodes, presented are the results of metallographic examinations of the deposited metal. Laboratory abrasive wear tests of composite alloys with experimental electrodes showed their high efficiency. 10 Ref., 1 Table, 2 Figures.

Keywords: *arc hardfacing, composite alloy, coated electrode, tungsten carbide, reinforcing particles, wear resistance*

The existing methods of producing composite alloys by the method of hardfacing are based on using the effect of reinforcement the deposited metal by particles of fused tungsten carbides WC + W_2C (relite), which have a high hardness (*HV* 1800–2200) and high specific weight. The most widespread method for producing composite alloys is a manual oxyacetylene surfacing with a filler metal. As a filler material, most often the strip or much rare the tubular-grain relite, developed at the E.O. Paton Electric Welding Institute, as well as rods or flexible cords of foreign companies, are applied [1–3]. In the recent years, plasma-powder and laser surfacing of composite alloys became widespread [4, 5]. At present, to a lesser extent, the induction or plasma surfacing is used with the addition of powder or strip electrode [6]. It is also known about the application of furnace method for production of composite alloys [1, 7]. However, a large volume of preparatory works, the use of low-temperature materials as a matrix and a high power consuming restrain the spreading of the mentioned method.

All the methods of surfacing mentioned above need stationary stations and specialized equipment. However, the problems with surfacing materials arise when it is necessary to strengthen the parts in field conditions and if disassembly of parts is difficult. In such cases, for arc semi-automatic or manual hardfacing of composite alloys only imported consumables are applied in Ukraine. As a rule, these are flux-cored wires, rods, electrodes, of well-known companies like DURUM, Castolin, Sulzer Metco Woka and others.

In this regard, the development of domestic electrode materials for arc hardfacing of composite alloys represents a hardfacing interest. The application of electric arc hardafing has a number of advantages over other methods: universality and simplicity of technological process; high efficiency as compared to gas surfacing; low energy consumption for hardfacing; wide range of control of basic parameters of hardfacing mode; opportunity for mechanization and automation of the hardfacing process. To realize the electric arc hardfacing method, it is necessary to develop the new domestic electrode materialss which provide the producing of composite alloys with preset high service characteristics. The maximum efficiency of such alloys is achieved due to the optimal concentration of a reinforcing phase, which determines the wear resistance of deposited metal and also serviceability of the matrix (wear resistance, crack resistance, porosity, etc.) to the highest extent. Moreover, the wear resistance of the produced alloys is also largely depends on chemical composition of matrix, which is determined by the degree of dissolution of tungsten carbide granules due to the diffusion of tungsten and carbon in welding pool during hardfacing. This also leads to decrease in the concentration of a

reinforcing phase and increase in brittleness of matrix due to formation of secondary complex iron-tungsten carbides [8, 9]. This is particularly pronounced in using of tungsten carbide granules produced by crushing the ingots. As a rule, such granules are subjected to plenty of cracks, have irregular shape and sharp angles which facilitates their high dissolution in liquid matrix melt.

The works on creation of technology of spraying the refractory compounds, carried out at the E.O. Paton Electric Welding Institute, allowed starting the industrial production of granules of fused tungsten carbides of spherical shape of almost all fraction compositions from 0.05 to 0.8 mm. The strength of spherical particles is 1.5–1.7 times higher than the strength of crushed grains of similar composition, and the microhardness after spraying grew to *HV* 2800–3000 [10]. Moreover, the investigations showed, that due to the spherical shape of reinforcing particles, it was possible to significantly decrease their dissolution in hardfacing and to reduce the transition of tungsten and carbon from reinforcing particles to the matrix. Thus, in gas hardfacing using strip relite with crushed reinforcing grains of 0.45–0.63 mm size, the average content of tungsten in the matrix of the composite alloy reaches 18–20 %, and with spherical reinforcing grains of the same size it reaches 11–12 % [10]. Thus, when developing a new electrode material, it was advisable to use spherical granules of tungsten carbide WC + W_2C as a reinforcing phase and, thus, to provide their minimal dissolution in welding pool.

It is known that the ratio between the content of reinforcing particles and binder alloy of the composite alloy is one of the determinating conditions for wear resistance of the alloy as a whole. This ratio depends on the type and structure of filler material, granulometric composition of reinforcing particles and should be in the range of 60–70 %, which provides the content of wear resistant phase in the deposited layer to about 40 % as to the volume and its high wear resistance. This ratio became a basis for the development of a new hardfacing electrode material.

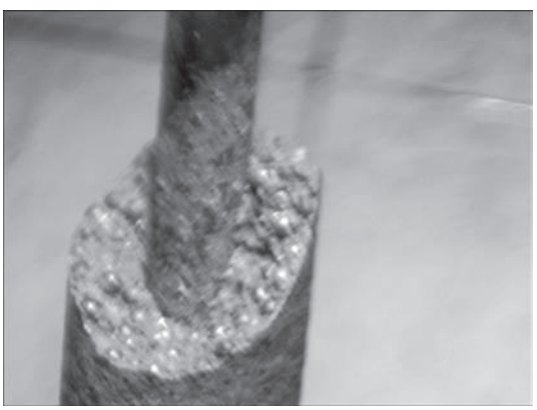

Figure 1. Electrode for electric arc hardfacing of composite alloys

The main feature of the designed electrodes is the fact that reinforcing granules are introduced to the composition of electrode coating, which, as a result, consists of the components considerably different between each other in size and specific weight of particles. This required the certain technological procedures in manufacture of electrodes of such composition in future. As a wear resistant component, the granulometric particles of tungsten carbides of spherical shape of 0.45–0.63 mm and 0.63–0.80 mm are applied. The selection of such particles is predetermined by design peculiarities of the equipment for manufacture of electrodes and the required coefficient of the coating mass.

The gas-slag-forming and alloying system is represented by traditional charge components applied for production of welding and surfacing materials. The granulometric composition of charge materials was in the range of 0.28–0.40 mm. As a gas-slag-forming system, the system based on marble and fluorspar concentrate was adopted. The deoxidation of welding pool was carried out by introducing ferromanganese and ferrosilicon into the electrodes coating composition. For a partial limitation of formation of brittle iron-tungsten structures in the matrix of deposited composite alloy, the doping ferroalloys, containing titanium and vanadium, are introduced into the coating composition.

These elements have a greater affinity to carbon than iron and tungsten, and, in the first turn, they form their carbides, thus reducing the amount of secondary iron-tungsten carbide phases. Taking into account the abovementioned difference in components as to their specific weight and granulometric composition, their mixing was carried out with keeping the necessary technological measures providing homogeneity of coating composition. At the same time, taking into account the high weight ratio of the coating, the electrodes shaping was carried out at the speeds considerably lower than the usual ones established for manufacture of typical electrodes. The ratio of weight of spherical particles of tungsten carbides in the coating to the weight of metallic rod was in the range of 60–65 %.

In the course of experiments, the modes of drying and calcination of electrodes after shaping were established, at which the corresponding quality of coat-

Results of tests of specimens on abrasive wear

Marking of specimen	Weight of specimen, g		Wear, g	Relative wear resistance
	Initial	After tests		
Steel 45-1	11.6157	10.9912	0.6245	1.0
OP-1	12.9226	12.8474	0.0752	8.3
OP-2	12.7251	12.6587	0.0664	9.4
OP-3	12.6434	12.5663	0.0771	8.1
Steel 45-2	11.8264	11.0612	0.7652	1.0
OP-4	13.0876	12.9895	0.0981	7.8
OP-5	13.3317	13.2485	0.0832	9.2
OP-6	12.9581	12.8659	0.0922	8.3
Steel 45-3	11.7361	11.0518	0.6843	1.0
S-1	12.6769	12.5869	0.0900	7.6
S-2	12.4935	12.3985	0.0950	7.2
S-3	13.1079	13.0058	0.1021	6.7

ing is provided. The calcination of electrodes should be carried out in vertical position using special yokes, as far as application of racks for drying in the horizontal position leads to a probable distortion in the uniformity of the electrode coating due to its high specific weight. The drying and calcination of electrodes is carried out according to the following cycle:

- drying of electrodes in the vertical position at a room temperature for 24 h;
- preliminary calcination of electrodes in the furnace at T = 200 °C for 1 h;
- calcination of electrodes in the furnace at T = = 400 °C for 2 h.

For comparative investigations, more than ten experimental compositions of filler materials were produced. The appearance of electrodes with particles of spherical tungsten carbides is shown in Figure 1.

To evaluate the technological features of hardfacing process by designed electrodes and metallographic examinations, the specimens were manufactured, deposited by these electrodes. Figure 2 presents macrostructure of the deposited composite layer. The concentration of reinforcing particles in the plane of the section amounts to higher than 45 %.

It should be noted that the process of hardfacing by new electrodes has its own technological features. The direct effect of arc on reinforcing particles can lead to their partial fracture, appearance of small particles of tungsten carbides and increase in the degree of saturation of matrix melt by tungsten and carbon.

In this regard, during hardfacing the application of technological procedures is required providing transition of tungsten carbides from coating to welding pool at a minimal effect of arc on the reinforcing particles. The hardfacing was carried out in flat position with a forward inclination of electrode at small oscillations, providing some delays in melting of coating and, thus, facilitating the transition of a significant part of reinforcing particles to welding pool, avoiding the region of high temperatures. However, the keeping of the mentioned procedures does not exclude the diffusion of tungsten and carbon into the binder alloy. Therefore, the complete exclusion of forming the undesired structures in the alloy matrix, which embrittle the matrix in the form of secondary iron-tungsten carbides and eutectics, is impossible. The results of investigations of microstructure of composite alloys produced by electric arc hardfacing will be covered in a separate work.

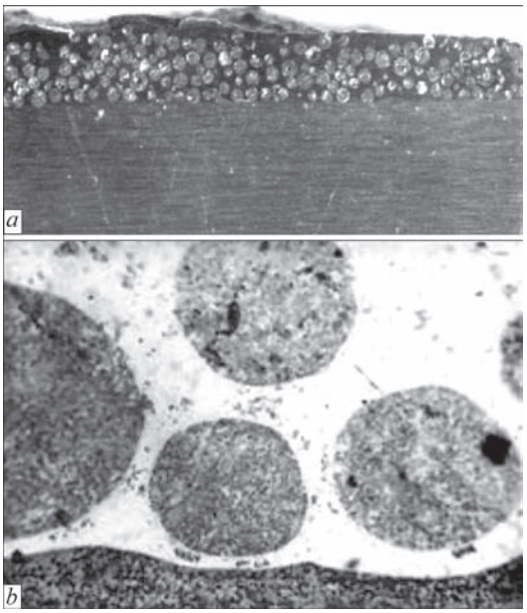

Figure 2. Macrostructure of composite alloy: *a* — ×80; *b* — ×200

To evaluate the wear resistance of composite layers deposited by experimental electrodes, the method of tests on abrasive wear in the machine NK-M was applied, which consisted in abrasion of specimens MI-90 moving along the copper path at the speed of 0.5 m/s under the load of 30 N. The friction path is 800 m, quartz sand serves as an abrasive. As a reference, the specimen of steel 45 is applied. The wear resistance is evaluated with respect to the weight loss of the reference specimen to the weight loss of the specimen tested. The test results are presented in Table. The data given in table show that the composite alloys deposited using experimental electrodes (OP-1–OP-6) are not inferior, and in some cases are 1.2–1.4 times superior to the serial ones (S-1–S-3) and can be successfully applied for wear-resistant hardfacing of different parts.

Conclusions

1. The electrodes for arc hardfacing of composite alloys were designed on the base of granular tungsten carbides of spherical shape, the feature of which is

the introduction of reinforcing granules into the coatings of electrodes. The designed electrodes provide concentration of reinforcing particles in the deposited composite layer of at least 40–50 %.

2. The technology for electrodes manufacture was developed, providing homogeneity of coating consisting of components different in specific weight and granulometric composition. The features of modes of drying and calcination of electrodes were determined.

3. The results of laboratory tests on abrasive wear allow predicting the high service characteristics of the developed electrodes.

1. Zhudra, A.P. (2014) Tungsten carbide based cladding materials. *The Paton Welding J*., **6–7**, 66–71.
2. (2016) Weld hardface and cladding material guide. *Oerlikon Metco*, **8**.
3. (2016) *Hard-facing materials*. DURUM Verschleiss-Schutz GmbH.
4. Harper, D., Gill, M., Hart. K.W.D., Anderson, M. (2002) Plasma transferred arc overlays reduce operating costs in oil sand processing. In: *Proc. of Int. Thermal Spray Conf*. (March 4–6, 2002, Essen, Germany). ASM International, 278–293.
5. Som, A.I. (2004) Plasma-powder surfacing of composite alloys based on cast tungsten carbides. *The Paton Welding J*., **10**, 43–47.
6. Bely, A.I. (2010) Influence of main technological parameters of the plasma cladding process on properties of composite deposited metal. *Ibid*., **6**, 25–27.
7. Danilov, L.I., Rovenskykh, F.M. (1973) Surfacing of parts of charging equipment of blast furnace by composite alloy. *Metallurg*, **1**, 18–21 [in Russian].
8. Frumin, E.I., Zhudra, A.P., Pashchenko, M.A. (1979) Physico-chemical processes in surfacing by strip relite. *Svarochn. Proizvodstvo*, **10**, 27–32 [in Russian].
9. Zhudra, A.P., Makhnenko, V.I., Pashchenko, M.A. et al. (1975) Peculiarities of automatic arc surfacing of composite alloys. *Avtomatich. Svarka*, **8**, 16–19 [in Russian].
10. Dzykovich, V.I., Zhudra, A.P., Bely, A.I. (2010) Properties of tungsten carbide powders produced by different technologies. *The Paton Welding J*., **4**, 22–24.

Received 28.11.2017

doi.org/10.15407/tpwj2018.01.07

INFLUENCE OF FLUX COMPOSITION ON THE PROCESS OF ELECTROSLAG SURFACING OF END FACES WITH DISCRETE FEEDING OF FILLER MATERIAL

Yu.M. KUSKOV
E.O. Paton Electric Welding Institute of the NAS of Ukraine
11 Kazimir Malevich Str., 03150, Kyiv, Ukraine. E-mail: office@paton.kiev.ua

Applicability of fluxes of different grades at electroslag surfacing of end faces by discrete filler material in a current-supplying mould was studied. It is found that selection of fluxes proceeding just from their physical properties (viscosity and electrical conductivity) does not guarantee the conditions required for conducting the electroslag process. Optimum position of the billet end face to be surfaced in the mould working cavity is very important for normal operation of the mould and performance of sound surfacing with good formation of the deposited metal. In view of the above-said, ANF-29, ANF-32, ANF-26 fluxes can be used for electroslag surfacing with discrete material. 20 Ref., 2 Tables, 4 Figures.

Keywords: *electroslag surfacing of end faces, flux, discrete filler, current-supplying mould, current, voltage, process stability*

Current-supplying mould (CSM) is a structure of sectioned type, combining the functions of nonconsumable electrode and device forming the deposited metal [1, 2]. It can be used both for electroslag surfacing (ESS), and electroslag remelting (ESR). Electrodes and billets of a large cross-section, wire, strip, solid and liquid fillers can be used as material fed into the liquid pool. Application of discrete filler seems to be the most promising, as it not only forms the deposited layer, but can have an inoculating impact on the solidifying metal structure.

Schematic of ESS of end faces with discrete filler in CSM is shown in Figure 1.

CSM is used as a mobile device, or it is mounted stationary with displacement of the layer being deposited relative to it. At deposition of relatively thin layers (approximately ≤90 mm) CSM can be used without relative displacement of the mould and the deposited metal. In this case the forming section of the mould should have the height which can accommodate the deposited layer. At layer thickness ≥90 mm, difficulties of heating the whole volume of the slag pool, arise, and metal formation becomes worse. Actual thickness of the layer with good formation is ultimately determined by physico-chemical properties of the applied flux, as well as the kind and chemical composition of the surfacing material. One of the main stages of conducting the electroslag process in CSM is setting the slag pool in it and preservation of its stability (stable chemical composition and specified electrical parameters of the process) during the entire period of CSM operation. The slag pool can be set in the mould with application of one of the two known techniques — liquid or solid start. In a regular mould, slag pool of optimum depth (40–100 mm) is formed by one-time pouring of the required portion of slag into it from flux-melting furnace, or the same slag volume is obtained by shorting the consumable or nonconsumable electrode on the tray (or billet being surfaced) with gradual increment of molten flux quantity, transferring the process form the arc to the slag one.

In CSM the poured-in slag portion can have different volume, depending on the position of the billet or tray, relative to current-conducting section of the

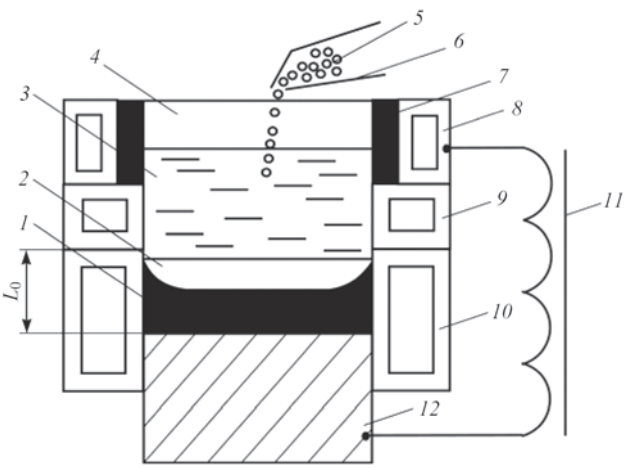

Figure 1. Schematic of ESS of end faces with discrete filler in CSM: *1* — deposited metal; *2* — metal pool; *3* — slag pool; *4* — mould; *5* — filler metal feed mechanism; *6* — discrete filler material; *7* — protective layer (molybdenum, tungsten and graphite); *8–10* — mould sections; *11* — transformer; *12* — billet

mould. The situation is similar also when performing the solid start, when the slag pool volume should be sufficient for closure of the electrical circuit of current-conducting section–slag–tray (or billet). This closure is exactly what allows ensuring CSM normal operation and conducting the electroslag process for a sufficiently long time without adding any additional devices or electrodes into the working zone for maintaining the slag pool in the molten state.

It should be also noted that, depending on the electric mode of surfacing and slag properties, the slag pool surface can vary considerably, and this, alongside the earlier mentioned influence of the slag pool thermal condition on surfacing quality, may lead to formation of non-conducting or partially current-conducting slag skull (solid or half-liquid crust) on the working surface of the current-conducting section, even in the case, when it is protected by electrically conducting lining, most often graphite one. Appearance of skull makes current passage through one of the working electric circuit elements difficult, process stability is disturbed; in the extreme case, the electroslag process stops completely.

Thus, correct selection of the flux (slag) is of paramount importance for normal CSM operation. Flux cost should be also taken into account. It is known that the flux cost is equal to 2–6 % in the cost of melting ESR ingots [3]. At ESS, when relatively small metal layers are mainly deposited, this value naturally becomes much greater.

From the moment of electroslag process invention at the end of 1940s – beginning of 1950s more than 50 flux grades have been proposed for its performance. The main component of the fluxes is calcium fluoride, characterized by the lowest vapour pressure at the temperatures of electroslag processes, compared to Al, Ba, Mg fluorides. Physical properties of molten CaF_2 ensure process stability.

Ca, Al, Mg oxides are added to reduce electrical conductivity, adjust melt viscosity, and improve its desulphurizing ability. Content of silica as a compound, which is less thermodynamically stable one than the above-mentioned oxides, and also lowers the desulphurizing ability of slag, is usually not higher than 2 %. However, at ring ESS, as well as in practical application of ESR, fluxes with increased silica content (ANF-14, ANF-25, ANF-28, ANF-29) are sometimes used.

At present, fluxes of different grades are used for conducting the electroslag process, depending on chemical composition of the metal being remelted, its kind and surfacing technique (in a mobile or stationary mould). The following examples of such an approach to selection of fluxes for operation with CSM can be given: ring ESS by liquid metal (chromium cast irons, stainless, tool, high-speed steels, etc.) with relative displacement of the deposited metal and mould with application of AN-75, ANF-32, ANF-94 fluxes [4–7]; remelting of electrodes and surfacing of end faces (titanium alloys, copper, low-alloyed and stainless steels) with CaF_2, ANF-94, ANF-28 fluxes [8–10]; ESR, end face and ring surfacing with feeding into the slag pool (ANF-14, AN-75, ANF-29, ANF-28N) discrete fillers (chromium and chromium-nickel cast irons, high-speed and die steels, copper, etc.) [4, 10–13].

The influence of some process parameters and chemical composition of fluxes on the stability of the electroslag process in CSM at ESS of end faces with discrete filler is considered in this work. In this case, alongside good formation of the deposited metal from the very start of surfacing and complete melting of the filler, it is also necessary to ensure sound joining of the base and deposited metal, using the correctly selected flux. The latter is a rather complicated task, compared, in particular, to ESR method, in which the removed (bottom) part of the ingot may reach 15 % of its weight [14]. Therefore, this task will be considered in the following papers.

Fluxes, which were accepted both in electroslag and in arc processes (AN-22, AN-26) were selected for preliminary consideration. Flux grades and their composition according to TU specification are given in Table 1.

Table 1. Fluxes, pre-selected for consideration of their applicability in the investigations

Flux grade	Chemical composition of fluxes, wt.%					
	CaF_2	Al_2O_3	CaO	SiO_2	MgO	MnO
ANF-14	60–65	10–12	≤ 8	14–16	4–8	–
ANF-29	37–45	13–17	24–30	11–15	2–6	–
ANF-32	34–42	24–30	20–27	5–9	2–6	–
ANF-94	34–40	17–21	11–22	14–20	7–11	≤ 2
AN-75	56–59	9–12	6–8	18–21	6–8	5–7
AN-90	39.0	10.5	23.5	26.5	0.5	–
AN-22*	20–24	19–23	12–15	18–22	12–15	7–9
AN-26	20–24	19–23	4–8	29–33	15–18	2.5–4

*Flux additionally contains $Na_2O + K_2O$ in the amount of 1.3–1.7 wt.%.

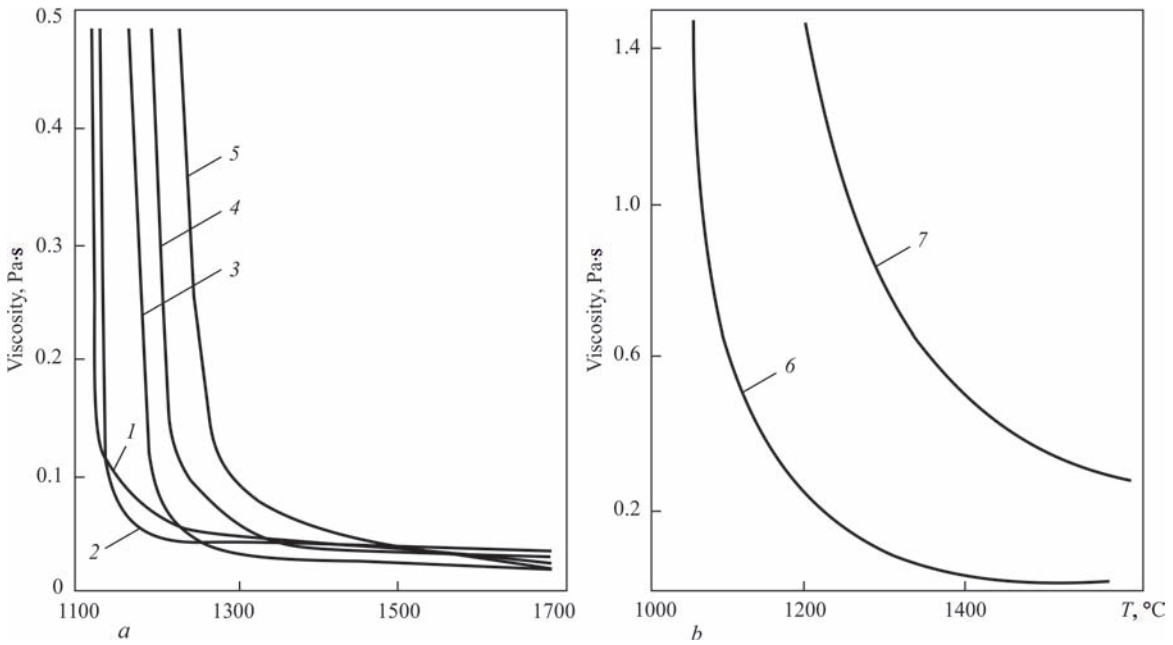

Figure 2. Dependence of flux viscosity on temperature [15–18]: *a* — salt-oxide; *b* — oxide fluxes: *1* — ANF-14; *2* — AN-75; *3* — ANF-29; *4* — ANF-32; *5* — ANF-94; *6* — AN-22; *7* — AN-26

Dependencies of the main physical characteristics of slags, namely viscosity and electrical conductivity, on temperature are given in Figures 2 and 3 [15–18]. There is no data on physical properties of AN-90 flux.

The main technical and economic characteristics of electroslag processes, and, accordingly, criteria for flux selection, were as follows:

Oxide-fluoride flux ANF-14 is used at electroslag welding of steels, as well as in ESS of cast irons, in particular, ESS by an electrode – pipe of hot rolling rolls [4]. At ESS with cast iron shot in CSM, slag inclusions were observed in the deposited metal and along the fusion boundaries of the base and deposited metal in a number of cases. This is associated with the cooling impact of shot fed into the slag pool, in contrast to that of overheated drops from the melted off consumable electrode tip. It is not produced commercially.

ANF-29 and ANF-32 fluxes are designed for ESS in mobile moulds, due to addition of an increased quantity of SiO_2 to their composition [19]. Presence of an increased content of silica in slag based on calcium fluoride, promotes producing a thin skull crust and good formation of the deposited surface in a wide range of variation of the melting modes. These fluxes are produced commercially.

ANF-29 flux. It was developed for ring ESS by liquid metal (high-speed steels) in CSM [10]. Similar to the case of ANF-14 flux, conditions of slag pool existence differ considerably at feeding the liquid and solid filler. It is not produced commercially.

AN-75 flux. It is a modification of ANF-14 flux due to addition of 5–7 % MnO to it. At ESS with cast iron shot in a mobile CSM, it provides good formation of cast iron and fusion of the base (steel, cast iron) and deposited metals [4]. At deposition of steel shot metal formation deteriorates, and unmolten shot particles occur in the deposited layer. It is not produced commercially.

AN-90 flux. It was developed for ESS by stainless steel strips with free formation of the deposited metal. It provides good metal formation, easy detachment of

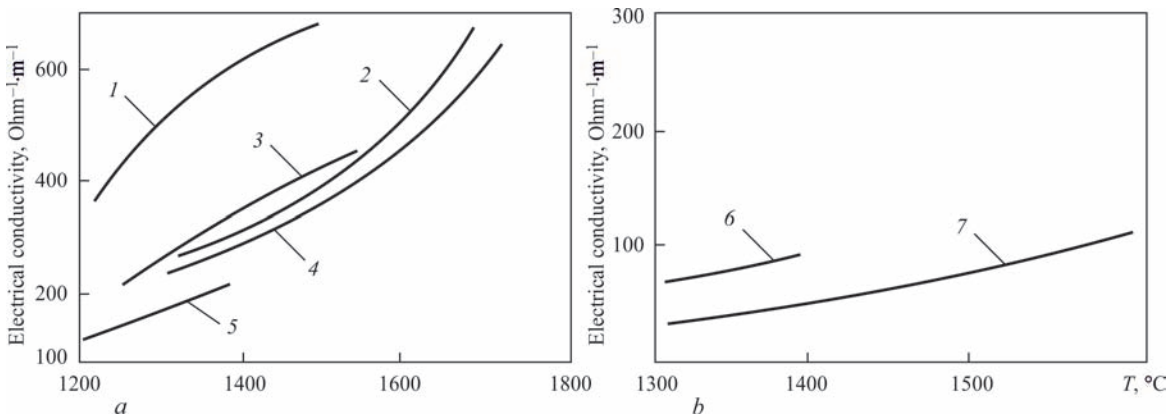

Figure 3. Dependence of flux electrical conductivity on temperature [15–18]: *a* — salt-oxide; *b* — oxide fluxes: *1* — AN-75; *2* — ANF-29; *3* — ANF-32; *5* — ANF-14; *6* — AN-22; *7* — AN-26

Table 2. Electrical characteristics (I, kA, U, V) of surfacing of end faces with discrete filler at certain position (L, mm) of the deposited layer

Flux grade	Measured parameters	Evaluation levels											
		1	2	3	4	5	6	7	8	9	10	11	12
ANF-29	L	0	88	82	76	70	64	58	52	46	40	34	28
	I	0.98	1.55	1.97	2.04	2.05	2.26	2.30	2.38	2.46	2.6	2.68	2.73
	U	62.6	59.2	57.0	56.6	56.4	55.6	55.5	55.1	54.7	53.8	53.5	54.4
ANF-32	L	0	88	82	76	70	64	58	52	46	40	34	28
	I	1.56	1.69	1.77	1.83	1.87	2.0	2.15	2.26	2.42	2.58	2.8	2.84
	U	34.5	43.8	42.6	42.6	41.5	40.0	37.6	34.4	34.2	31.2	30.2	27.3
AN-26	L^*	0	65	60	55	50	45	40	35	–	–	–	–
	I	2.33	2.44	2.54	2.56	2.72	2.83	2.95	3.16	–	–	–	–
	U	57.3	57.2	56.6	56.6	55.6	54.8	54.5	53.4	–	–	–	–

*L_0 = 70 mm.

the slag crust, maintaining a stable electroslag process at a small depth of the slag pool, low susceptibility to hydratation [20]. It is not commercially produced.

AN-22 flux. It is used both for electric arc welding, and for high-alloyed steel surfacing. A relatively low content of highly deficit CaF_2 can be regarded as the advantage of this flux. It is not produced commercially.

AN-26 flux. Its application and advantages are similar to those of AN-22 flux. It is produced commercially in the vitreous variant (AN-26S).

As a result of the performed analysis, ANF-29, ANF-32, AN-90, AN-22 and AN-26 fluxes were selected for investigations. Application of AN-90 and AN-22 fluxes caused the greatest doubt. The first one — for the reason of lack of understanding of its behaviour at ESS in water-cooled moulds, the second one — because of presence of about 2 % of sodium and potassium oxides in its composition, that supposedly would hinder preservation of their content during surfacing.

In this connection, investigations were divided into two stages. At the first stage practical verification of stabilization of electroslag process with AN-22 and AN-90 fluxes was performed at ring ESS in CSM with a widened upper section and increased diameter of the surfaced billet. Such a surfacing schematic allowed reducing the slag pool volume (2870 cm^3) to improve its preheating conditions. But in this case, too, after pouring each of these slags into the mould (liquid start), it was not possible to set a stable slag pool, even at maximum level of the power source.

Figure 4. Appearance of side surface of the deposited layer with application of AN-26 flux at initial value of L_0 equal to 70 mm (longitudinal section of the deposited billet)

Therefore, the main investigations (stage 2), were conducted with application of ANF-29, ANF-32 and AN-26 fluxes at surfacing of end faces in a smooth-bore CSM with 3820 cm^2 volume of the slag pool (approximately by 30 % greater than in experiments of the 1st stage). Procedure of experiment performance was as follows (see Figure 1). In CSM of 180 mm diameter, the water-cooled electrode with a graphite attachment at its end was used to set a slag pool on the billet surface, by successively melting flux portions, until the pool began touching the current-conducting section of the mould. From this moment, CSM operation began, and the electrode was removed from its working cavity. After preheating the slag pool for three minutes, dry fine chips (after milling) of the following chemical composition, wt.%: 0.50 C; 0.62 Si; 1.3 Mn; 3.30 Cr; 0.93 Ni; 0.15 Mo; ~ 1.0 Cu, were fed into it in portions. Prior to that, chips weight to which a certain deposited layer thickness corresponds, was determined. All the surfacing operations were performed at the maximum IV level of transformer TShP-10. Initial distance from the processed surface of the billet to the upper edge of the forming section (L_0) was equal to 94 mm.

During surfacing, maximum possible distance from the processed surface of the billet to the edge of forming section (L_0) was determined for each flux (from evaluation levels), as well as currents and voltages, corresponding to each position of the deposited metal level.

Results of the performed experiments are shown in Table 2. Analysis of measurement results, technological features of surfacing operations, as well as the values of viscosity and electrical conductivity of fluxes depending on temperature (Figures 2, 3), lead to the

following conclusions. Despite the relatively close values of physical properties of ANF-29 and ANF-32 fluxes, their behaviour at surfacing is different. Each feeding of steel chips into the slag pool reduced the distance from the deposited layer surface to the current-conducting section, thus lowering the electrical resistance in the section-slag-deposited metal segment. Here current rises and for ANF-29 flux, approximately at the third evaluation level, the slag pool already actively rotates in the horizontal plane, quietly absorbing the fed portions of the filler. At application of ANF-32 flux, the weight of the first portions of chips had to be minimized, as the thermal power of the slag pool was insufficient for melting large portions of filler. When attempting to increase their mass feed rate, the chips significantly impaired the process stability, because of lowering of slag temperature. And only after achievement of approximately level 4–5 the process was completely stabilized. Therefore, for ANF-32 flux the initial L_0 value should be equal to about 70–75 mm.

Considering the physical properties of AN-26 flux (relatively low electrical conductivity, increased viscosity and melting temperature), it was decided to conduct the experiments at initial value L_0 = 70 mm. For these surfacing conditions the slag pool formed due to melting of AN-26 flux, is set without any difficulties, even at level II of the power source. At surfacing proper (level IV of the power source) the chips were actively melting in the slag, which had a higher temperature at visual evaluation. Correctness of selection of initial value L_0 was confirmed by that the side surface of the deposited layer, corresponding to feeding chips on level 1–2, was slightly worse formed than on the other levels (Figure 1).

Conclusions

1. At ESS of end faces with discrete filler in CSM the specific conditions of CSM operation make special requirements not only to physical properties of fluxes, but also to laying out the mould working space (arrangement of the billet to be surfaced in it).

2. Selection of fluxes proceeding just from their physical properties, does not guarantee optimum conditions of conducting the electroslag process at ESS in CSM.

3. «Long» ANF-29 and ANF-32 fluxes are suitable for performing ESS of end faces in both mobile and stationary CSM. «Short» AN-26 flux can be used in the technologies of surfacing without relative displacement of the mould and surface billet. In both the cases, stable electroslag process and good formation of the deposited metal are ensured at optimum positioning of the processed end face in CSM working cavity.

1. Ksyondzyk, G.V. (1975) Current-supplying mold providing rotation of slag pool. *Spets. Elektrometallurgiya*, **27**, 32–40 [in Russian].
2. (1980) Frumin, I.I., Ksyondzyk, G.V., Shirin, V.S. (1980) *Welding apparatus for electroslag remelting and surfacing*. Pat. 4185628 USA [in Russian].
3. Glebov, A.G., Moshkevich, E.I. (1978) *Electroslag remelting*. Moscow, Metallurgiya [in Russian].
4. (2015) *Surfacing. Technologies, materials, equipment*: Transact. Kiev, PWI [in Russian].
5. Medovar, L.B., Chernets, A.V., Grabovsky, Ts.F. et al. (2000) Experience of manufacture and application of high-speed rolls of ESS LM. *Problemy Spets. Elektrometallurgii*, **3**, 3–9 [in Russian].
6. Medovar, B.I., Tsykulenko, A.K., Medovar, L.B. et al. (1997) Electroslag processes without consumable electrodes. *Ibid*., **2**, 12–16 [in Russian].
7. Medovar, B.I., Saenko, V.Ya., A.K., Medovar, L.B. (2000) Manufacture of billets of corrosion-resistant bimetal by electroslag surfacing method. *Ibid*., **2**, 3–11 [in Russian].
8. Medovar, L.B., Bents, M.J. (1998) Current-supplying mold for electroslag refining of titanium alloys with independent control of slag temperature, speed of slag rotation and speed of electrode melting. *Ibid*., **4**, 13–15 [in Russian].
9. Zajtsev, V.A., Medovar, L.B., Tishchenko, P.I. et al. (2011) Application of ESR by a two-circuit scheme for obtaining steel-copper billets of anodes of DC arc furnaces. *Sovrem. Elektrometall*., **2**, 3–7 [in Russian].
10. Medovar, L.B., Tsykulenko, A.K., Chernets, A.V. et al. (2000) Examination of influence of two-circuit scheme parameters of ESR on dimensions and shape of metal pool. *Problemy Spets. Elektrometallurgii*, **4**, 3–7 [in Russian].
11. Kuskov, Yu.M. (2003) A new approach to electroslag welding. *Welding J*., **4**, 42–45.
12. Kuskov, Yu.M., Beskorovajny, V.I., Us, V.I., Medovar, L.B. (1992) Electrodeless electroslag technology of copper wastes remelting. *Problemy Spets. Elektrometallurgii*, **3**, 29–32 [in Russian].
13. Kuskov, Yu.M., Gordan, G.N., Bogajchuk, I.L. et al. (2015) Electroslag surfacing using discrete materials of different methods of manufacture. *The Paton Welding J*., **5–6**, 30–33.
14. Latash, Yu.V., Medovar, B.I. (1970) *Electroslag remelting*. Moscow, Metallurgiya [in Russian].
15. Medovar, B.I, Tsykulenko, A.K., Shevtsov, V.L. et al. (1968) *Metallurgy of electroslag process*. Kiev, Naukova Dumka [in Russian].
16. Podgaetsky, V.V., Kuzmenko, V.G. (1988) *Welding slags*: Welding manual. Kiev, Naukova Dumka [in Russian].
17. Kozin, R.V., Grigorenko, G.M. (2016) Physical-chemical properties of fluxes for electroslag technologies. *Sovrem. Elektrometall*., **4**, 10–15 [in Russian].
18. Istomin, S.A., Pastukhov, E.A., Denisov, V.M. (2009*) Physical-chemical properties of oxide-fluoride melts*. Ekaterinburg, Ur ORAN [in Russian].
19. Artamonov, V.L., Medovar, B.I., Likhacheva, T.N. et al. (1976) New fluxes ANF-28, ANF-29 and ANF-32 for ESR in movable molds. *Spets. Elektrometallurgiya*, **30**, 33–38 [in Russian].
20. Kalensky, V.K., Panchishin, Yu.A. (1990) *Materials and equipment for corrosion-resistant electroslag surfacing with two electrode strips*: Transact.: Equipment and materials for surfacing. Kiev, PWI, 96–100 [in Russian].

Received 12.09.201

doi.org/10.15407/tpwj2018.01.08

INTERNET DATABASE OF ARC SURFACING PROCESS USING FLUX-CORED WIRES

V.G. SOLOVIOV
E.O. Paton Electric Welding Institute of the NAS of Ukraine
11 Kazimir Malevich Str., 03150, Kyiv, Ukraine. E-mail: office@paton.kiev.ua

A significant volume of work was performed on arc surfacing with application of self-shielded flux-cored wire on flat and cylindrical surfaces of workpieces by an open arc, submerged arc and in shielding gas atmosphere, in a wide range of voltages and currents of the arc, with different wire diameters and at different deposition rates, in order to use the experimental material to develop algorithms for automation of the technological process. The paper presents a solution on systematization of the data, obtained as a result of experiments, which allowed all the investigation participants to have remote access to the Internet database for its expansion, correction and analysis. 8 Ref., 3 Figures.

Keywords: *automation, database, arc surfacing, flux-cored wire*

Integrated automation of nonlinear multifactorial technological process of arc surfacing of metals requires involvement of considerable mathematical and computational resources on modeling relations of a large number of parameters, part of which can be obtained using sensors, and the other part by indirect method, using the apparatus of regression analysis, neural network technologies, fuzzy logic, etc. In addition to that, optimization of the process is contemplated, and in this case optimization will be multicriterial, that greatly complicates system synthesis. Recently, the synergetic principles of synthesis [1] are ever more often used for automation of «dissipative systems», to which the arc process belongs. These principles allow stabilizing the relationships between the variable states of the process. The consequence of this fact is degeneracy of the equations of dynamics of arc surfacing process and presence of integral invariants of manifolds in the space of its states. Invariant manifolds represent «certain functions which do not change during movement» [2]. Such approaches to automation of nonlinear objects greatly simplify the system synthesis and can be used for reaching the ultimate automation goals, i.e. improving the manufactured product quality with maximum energy saving. However, they require conducting a considerable number of experiments for analysis. A large scope of experimental arc surfacing with flux-cored wire of flat and cylindrical surfaces of products has been performed to obtain data characterizing the arc surfacing process, which furtheron will be used for analysis and synthesis of an automation system. Open-arc, submerged-arc and gas-shielded arc surfacing was performed in a broad range of voltages and currents of the arc with different diameters of flux-cored wire and at different deposition rates. Quality characteristics of the deposits and deposited beads were obtained, which are particularly significant for process automation.

The objective of this work is compiling an Internet database of the results of experimental arc surfacing with flux-cored wires for remote sharing during development of a system of automatic regulation of arc surfacing process.

Figure 1 shows a list of input and output data of the process of arc surfacing. The following process parameters are input data for the process: kind of surfacing (open-arc, submerged-arc or gas-shielded surfacing), flux-cored wire grade and its diameter, electrode extension, deviation from the item equator (for surfacing on cylindrical surface), etc. Controlling parameters are the position of manual device for setting power source voltage, position of manual device for setting electrode wire feed and position of manual device for setting the deposition rate on the unit control panel.

During preparation for experiment performance, software was developed within the framework of automated acquisition of statistical data [3], which provided monitoring and digital recording of the following parameters of arc surfacing process:

- instantaneous values of power source voltage $U_{p.s}(t)$;
- instantaneous values of surfacing current $I_s(t)$;
- $U_{p.s}(t)$ and $I_s(t)$ values average over surfacing time;
- instantaneous values of arc voltage $U_a(t)$ and arc current $I_a(t)$; here $U_a(t)$ and $I_a(t)$ values were determined by excluding from $U_{p.s}(t)$ and $I_s(t)$ values the voltage and current values in the time intervals of appearance of short-circuits (ShC) and arc breaks;
- arc voltage and arc current values average over surfacing time;
- manual entering and recording of settings of arc voltage and current voltage;

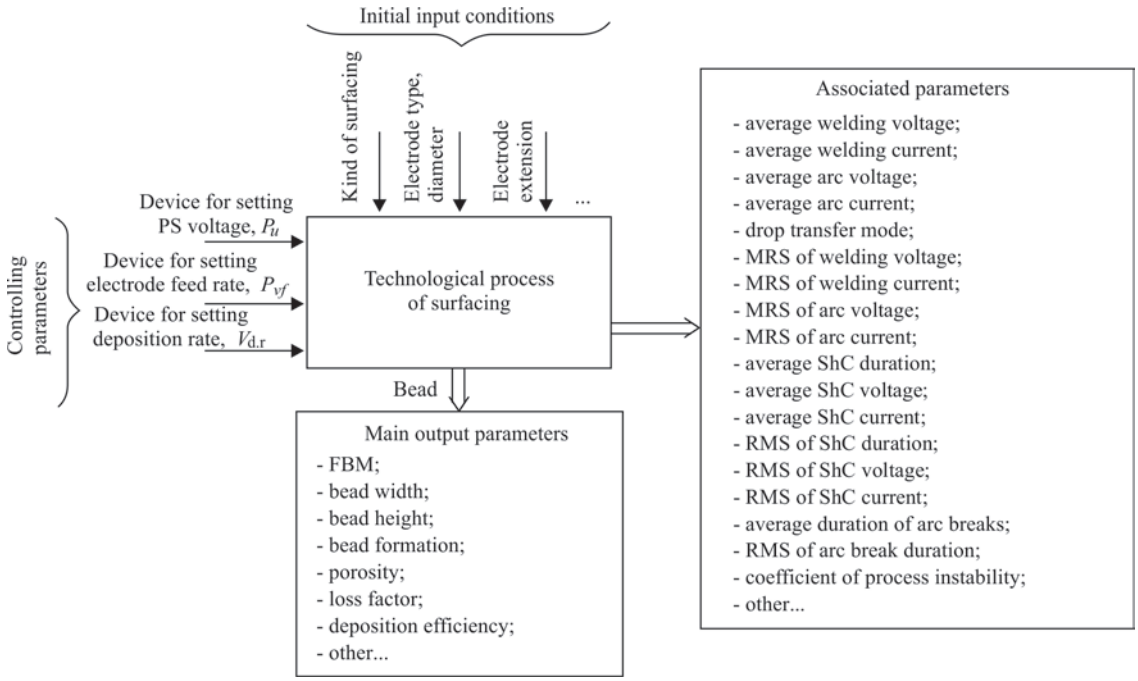

Figure 1. List of input and output data of the technological process of arc surfacing

● manual entering and recording of values of the position of manual device for setting power source voltage P_u, position of manual device for setting electrode wire feed rate P_{vf} and deposition rate $V_{d.r}$;

● ShC duration average over surfacing time;

● ShC voltage average over surfacing time;

● ShC current average over surfacing time;

● duration of arc breaks average over surfacing time;

● calculation and recording of such statistical parameters as MRS (mean-root-square error) value of welding voltage and arc voltage; MRS value of welding current and arc current; MRS value of ShC duration, voltage and current; MRS value of arc break duration;

● coefficient of instability of electric parameters of surfacing;

● type of metal drop transfer: globular, drop, fine-drop or spray;

● calculation and recording of evaluation by average duration of arc breaks. The following states were determined: «no breaks», «allowable number of breaks», «considerable number of breaks», «many breaks», «a great number of breaks» or «process is unstable».

During experiments, surfacing time, kind of surfacing, flux-cored wire grade, wire diameter, electrode extension, kind of workpiece surface, deviation from zenith of a cylindrical billet were recorded. Deposited beads were photographed, and time chart entries were recorded by such parameters as instantaneous welding voltage and welding current, instantaneous arc voltage and arc current.

At the end of each surfacing operation surfacing protocol was automatically generated in the form of a text file.

Results of expert evaluation of the deposited beads were used to determine the quality of bead formation as: «poor», «satisfactory» or «good»; presence of pores: «no pores», «individual pores» or «numerous pores».

Processing macrosections yielded such parameters as: «fraction of base metal in the deposited metal» (FBM); bead cross-sectional area, bead width, bead height and penetration.

Analysis and processing of experimental results yielded a lot of data on interconnection of various parameters, regularities of their change, depending on initial input conditions. This was recorded [3, 4] in the form of various graphs, figures and tables.

It resulted in obtaining data on arc surfacing of about 250 experimental beads, each of which is characterized by about 50 values of the above parameters unique for each bead, i.e. approximately 12500 data points [3]. By their structuredness, these data completely correspond to the definition of normalized relational database [5, 6], i.e. these data can be placed in a two-dimensional table, in which the relationships between information are fully defined. Marking the deposited bead is the primary KEY for such a table. Unique parameters, inherent to just this bead, are placed in the table rows in the corresponding cell. Markings are stamped on the item near the bead with shock markers for metal so that the marks did not disappear at further cutting and processing of the items. The database has the following structure: OBJECT is the bead; ATTRIBUTES are all the above-listed parameters, characterizing the deposited bead. In the Table the number of rows (entries) corresponds to the number of deposited beads, and the number of columns (fields) corresponds to the number of attributes.

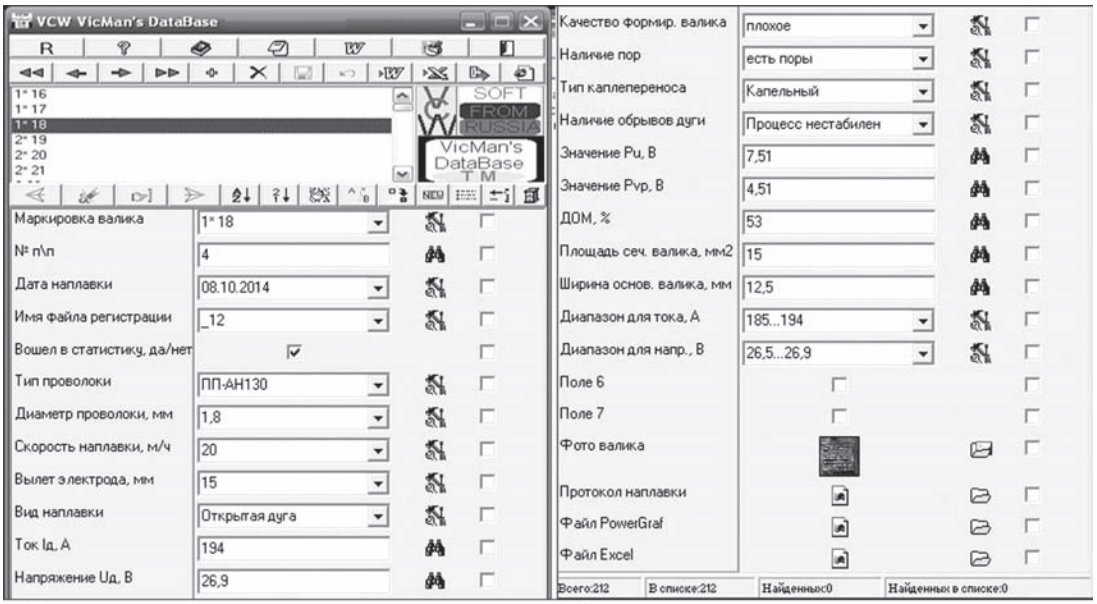

Figure 2. Arc surfacing database created using VCW VicMan's DataBase

Known are examples of databases of the modes of CO_2 arc welding, submerged-arc and inert-gas arc welding [7], which were developed on the basis of specialized software, suitable for application for the range of products, characteristic for this machine-building plant, and only within this plant. This software, however, is not suitable for collective study of the technology of self-shielded flux-cored wire arc surfacing with the purpose of process automation. Figure 2 shows the main form of the control system of VCW VicMan's DataBase (further on DBCS) which we used initially for systematizing and integrating (in the form of surfacing database) all the data derived as a result of experiments. DBCS is simple and very flexible for creation of small relational databases. It allows creating up to seven types of fields (text, graphic file of any format, in the form of a list, in the form of a flag, etc.). It allows editing the database, exporting it into a file and importing it from a file. It searches the text fields and sorts the entries in the required order; exports the database into Microsoft Word, Excel, into DBF and HTML format files. It, however, has a limitation by the number of fields — up to 30 ones (in this case about 50 or more are required). Here, as shown by practical work with the surfacing database, it is very often necessary to perform computations, using the data in the tables, for instance, determine the sum of the selected data, determine the value of autocorrelation or cross-correlation coefficients. However, this DBCS does not have such a capability. Therefore, it is necessary to export data into Excel program, which has a sufficient arsenal of tools for analysis, computation and visualization, and to perform the required computations in this program. Moreover, VCW VicMan's DataBase cannot be placed in the cloud Internet resource, and without it, under the present conditions, it is impossible to organize efficient collective research on the defined problem. For its filling and analysis the arc surfacing database requires participation of different groups of experts, specializing in certain areas of the work on the defined problem. And this work should be performed from different workplaces.

Internet database (cloud database, web-database) is the electronic distributed database, accessible through the Internet, unlike the lumped databases, accessible only in an individual computer or on the storage device connected to it, for instance, compact disc. Such databases are located on servers, fitted with a web-interface that allows access to them using widely accepted software through one of the public web-browsers. Intensive introduction of services for cloud computations by providers, led to Internet-databases becoming increasingly in demand. Such services, as Amazon Web Services (AWS), Google Cloud SQL, Microsoft Azure, SAP, Oracle, etc, operate in the cloud database market. They are attractive for customers with bases having a large distributed volume of data, for whom such cooperation is cost-effective.

A relational database can also be created in Microsoft Excel software package. In this case, Excel will perform, in some sense, the role of DBCS uncharacteristic for it, but, nonetheless the one it often plays [8]. If the relational database created in Excel, is not normalized, i.e. has several values in one cell of the table, then an additional table has to be compiled, which is linked to the first one, that complicates working with Excel as the database control system. Now in

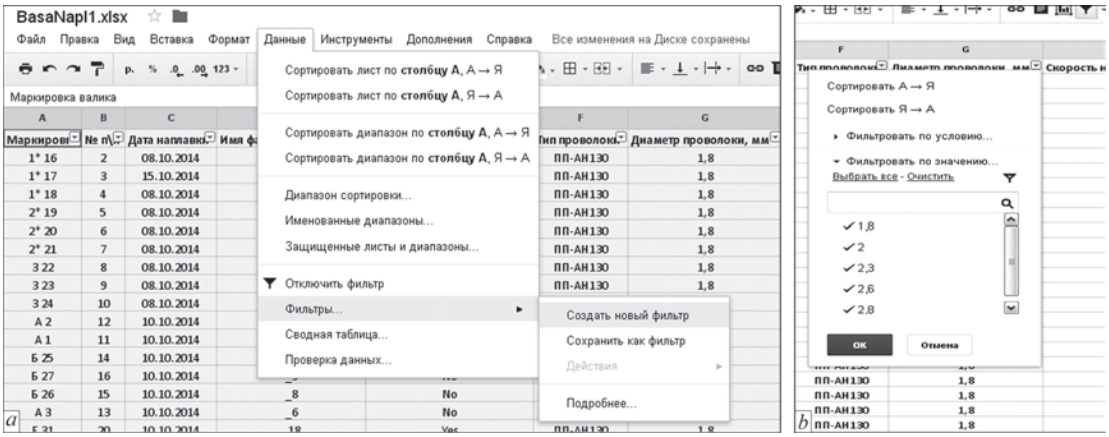

Figure 3. Some database functions, realized in Google Tables: *a* — sorting function; *b* — filtering function

our case, the surfacing database is normalized, and it can be placed in one table. Moreover, if required, hyperlinks to a graphic, text or other document, as well as the executed file, can be entered in the table fields that is very convenient, but searching by these fields is impossible in Excel.

At present Google Drive cloud resource provides for free use of more than 15 GB of cloud memory for secure file storage, including Microsoft Word, Excel documents, photos and videos. Thus, it enables other users looking through, editing and copying the documents. Google Tables application allows working with Excel files quite comfortably, practically no worse than in Microsoft Office Excel. It is possible to work not only on-line, but also off-line with subsequent synchronizing with Google Tables, when you turn on the Internet, as well as to work on the smartphone, with installed OS Android 4.0 and later versions. Moreover, Google Tables supports simultaneous joint work with tables of an unlimited number of employees, who received the right of access from the administrator.

Cloud database of arc surfacing results, created in Google Tables, allows editing, managing, and sorting the data (Figure 3, *a*), filtering it by columns (Figure 3, *b*), as well as generating reports based on data stored in spreadsheets. Results can be manually entered into the database, or imported into the Google Tables. If the data pertain to other programs, then before importing, they should be saved in Excel format, and after that imported into Google Tables. Google Tables application allows computing the result by the most diverse criteria:

- sum — data is summed;
- count — number of cells in the numerical range is counted;
- average value — mean arithmetic value is calculated for the selected data range;
- minimum and maximum values — shows the lowest and the highest values in the selected range;
- product — calculates data product;
- standard deviation — assesses the standard deviation in a sample;
- dispersion — assesses the dispersion in a sample, etc.

Conclusions

1. Capabilities of Google Tables Internet resource for creation of a fully functional cost-effective database of arc surfacing process for shared use were studied and confirmed.

2. An Internet database of the results of the process of experimental arc surfacing with flux-cored wires was created for its remote sharing in order to develop an automatic system of regulation of arc surfacing process.

1. Kolesnikov, A.A. (1994) *Synergic control theory*. Taganr. TRTU. Moscow, Energoatomizdat [in Russian].
2. Vladimirsky, E.I., Ismajlov, B.I. (2011) *Synergic methods of chaotic system control*. Baku, ELM [in Russian].
3. Ryabtsev, I.A., Lankin, Yu.N., Soloviov, V.G. et al. (2015) Computer information-and-measuring system for investigation of arc surfacing processes. *The Paton Welding J*., **9**, 32–35.
4. Lankin, Yu.N., Ryabtsev, I.A., Soloviov, V.G. et al. (2014) Effect of electric parameters of arc surfacing using flux-cored wire on process stability and base metal penetration. *Ibid*., **9**, 25–29.
5. Connolly, T., Begg, C., Strachan, A. (2001) *Databases: Design, implementation and management. Theory and practice*. Moscow; St.-Petersburg; Kiev, Williams [in Russian].
6. Redmond, E., Wilson, J.P. (2013) *Seven databases in seven weeks. Introduction in current databases and NoSQL ideology*. Ed. by J. Carter. Moscow, DMK Press [in Russian].
7. Demchenko, V.F., Kozlitina, S.S. (2010) Database of modes of CO_2-, flux-cored and inert gas arc welding. *Izvestiya TulGU. Tekhnicheskie Nauki*, 4, 1 [in Russian].
8. Dolzhenkov, V.A., Stuchenkov, F.B. (2007) *Microsoft Office Excel 2007*. St.-Petersburg, BKhV-Petersburg [in Russian].

Received 21.11.2017

UNIT FOR HIGH-VELOCITY ELECTRIC ARC SPRAYING

> The unit is designed for deposition of wear, corrosion resistant and special coatings, repair of worn machine parts by means of double-wire electric arc spraying in high-velocity flow of hot combustion products of hydrocarbon gas with air of current-conducting materials in form of wire (flux-cored wire) of 1.6–2.2 mm diameter. Joint development of PWI and «PLAZER» Company.

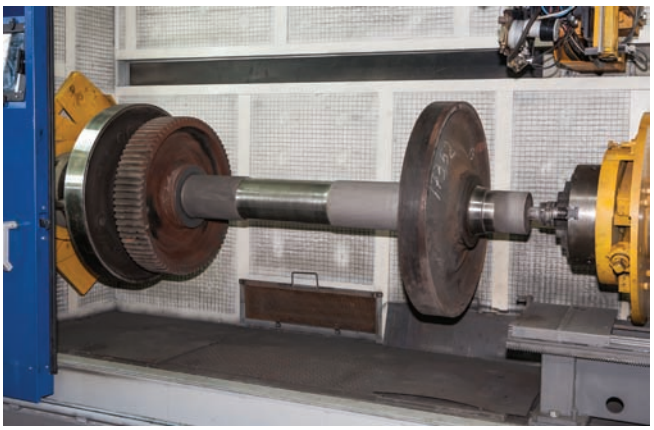

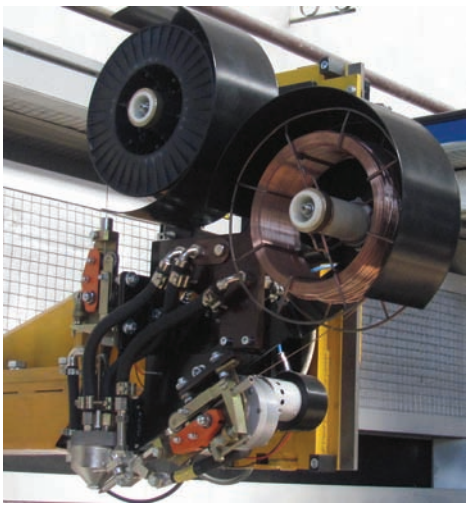

Block of high-velocity electric arc metallizer

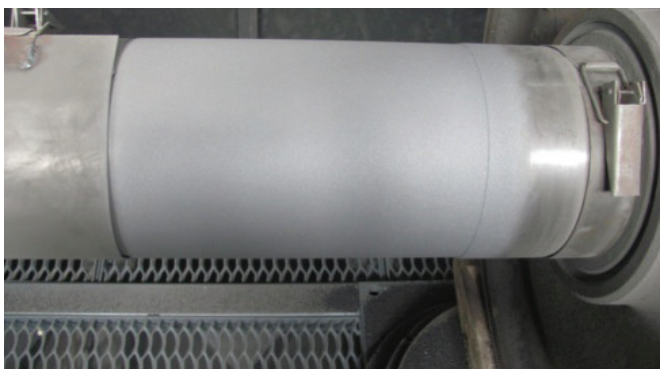

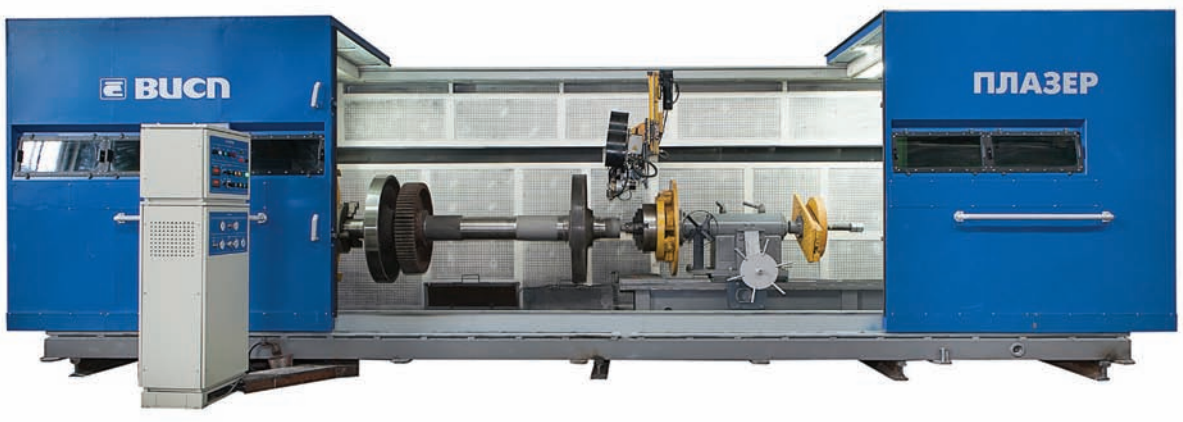

Appearance of restored part and unit in the framework of semi-automatic line

Developed by the E.O. Paton Electric Welding Institute of the NAS of Ukraine. E-mail: office@paton.kiev.ua

INDUCTION HIGH-FREQUENCY UNIT
FOR REMELTING OF REFRACTORY POWDER MATERIALS

One of the perspective directions of HF-plasma application is remelting of powder materials. A source of HF-discharge is a high-frequency generator, which induces a powerful electromagnetic high-frequency field in the inductor. The inductor contains a plasmatron forming a set mode for plasma forming gas escape at 7000–10000 °C temperature.

One of the directions of HF-plasma application is remelting of powder materials with further deposition of molten particles on a substrate; the second one is remelting and balling of powder materials. High melting efficiency of oxide materials allows wide application of developed equipment in additive technologies.

- Technology of plasma treatment of powder materials using HF-plasma allows receiving the spherical particles independent on shape of raw material. Application of special design reactor allows treatment of powder of chemically active metals and alloys in plasma with their further usage for additive technologies.

Joint development of PWI and «PLAZER» company.

PATON PUBLISHING HOUSE

www.patonpublishinghouse.com

SUBSCRIPTION

«The Paton Welding Journal» is Published Monthly Since 2000 in English, ISSN 0957-798X, doi.org/10.15407/tpwj.

«Avtomaticheskaya Svarka» Journal (Automatic Welding) is Published Monthly Since 1948 in Russian, ISSN 005-111X, doi.org/10.15407/as.

«The Paton Welding Journal» is Cover-to-Cover Translation of «Avtomaticheskaya Svarka» Journal into English.

If You are interested in making subscription directly via Editorial Board, fill, please, the coupon and send application by Fax or E-mail.

The cost of annual subscription via Editorial Board is $348 for «The Paton Welding Journal» and $180 for «Avtomaticheskaya Svarka» Journal.

«The Paton Welding Journal» can be also subscribed worldwide from catalogues subscription agency EBSO.

SUBSCRIPTION COUPON

Address for journal delivery _____

Term of subscription since _____ **20** **till** **20** _____

Name, initials _____

Affiliation _____

Position _____

Tel., Fax, E-mail _____

We offer the subscription all issues of the Journals in pdf format, starting from 2009.

The archives for 2009–2016 are free of charge on *www.patonpublishinghouse.com* site.

ADVERTISEMENT

in «Avtomaticheskaya Svarka» and «The Paton Welding Journal»

External cover, fully-colored:
First page of cover (190×190 mm) — $700
Second page of cover (200×290 mm) — $550
Third page of cover (200×290 mm) — $500
Fourth page of cover (200×290 mm) — $600

Internal cover, fully-colored:
First/second/third/fourth page of cover (200×290 mm) — $400

Internal insert:
Fully-colored (200×290 mm) — $340
Fully-colored (double page A3) (400×290 mm) — $500

- Article in the form of advertising is 50 % of the cost of advertising area
- When the sum of advertising contracts exceeds $1001, a flexible system of discounts is envisaged

Size of journal after cutting is 200×290 mm

Editorial Board of Journals «Avtomaticheskaya Svarka» and «The Paton Welding Journal»
E.O. Paton Electric Welding Institute of the NAS of Ukraine
International Association «Welding»
11 Kazimir Malevich Str. (former Bozhenko Str.), 03150, Kiev, Ukraine
Tel.: (38044) 200 60 16, 200 82 77; Fax: (38044) 200 82 77, 200 81 45
E-mail: journal@paton.kiev.ua; www.patonpublishinghouse.com